

Microgrids to support Communication Infrastructure

DESIGN DOCUMENT

Team 46, May 2021

Client/Advisor: Anne Kimber

Team Members: Liam McAlister, Hoang Dang, Dylan Miley,
Abdelrahman Mannan, Ryley Radack

Website: <https://sdmay21-46.sd.ece.iastate.edu/>
sdmay21-46@iastate.edu

Revised: April 22/v0.4

Executive Summary

Development Standards & Practices Used

- Matlab/Simulink simulation
- IEEE 1547: IEEE Standard for Interconnection and Interoperability of Distributed Energy Resources with Associated Electric Power Systems Interfaces
- IEEE 1526: IEEE Recommended Practice for Testing the Performance of Stand-Alone Photovoltaic Systems

Summary of Requirements

- Design and simulate in Simulink/Matlab a microgrid system that solely utilizes renewable generation and storage components:
 - Solar panel
 - Hydrogen fuel cell
 - Wind turbine
 - Battery
 - Inverters
- Each member of the team should develop familiarity with testing and evaluating different components:
 - Testing of hydrogen fuel cell
 - Testing of solar panel and battery.

Applicable Courses from Iowa State University Curriculum

- EE 303: Energy Systems and Power Electronics
- EE 456: Power System Analysis I
- EE 457: Power System Analysis II
- EE 459: Electromechanical Wind Energy Conversion and Grid Integration
- EE 475: Control System Simulation

New Skills/Knowledge acquired that was not taught in courses

- Wind/solar data gathering.
- Microgrid simulation
- Inverter design
- Project Planning/Management
- Hydrogen fuel cell testing station operation.

Table of Contents

1 Introduction	7
1.1 Acknowledgement	7
1.2 Problem and Project Statement	7
1.2.1 Problem Statement	7
1.2.2 Project Statement	7
1.3 Operational Environment	7
1.4 Requirements	8
1.5 Intended Users and Uses	8
1.6 Assumptions and Limitations	8
1.6.1 Assumptions:	8
1.6.2 Limitations:	8
2 Project Plan	8
2.1 Task Decomposition	8
2.2 Other Resource Requirements	9
2.3 Financial Requirements	9
2.4 Project Plan Changes	9
2.4.1 Additions To The Project Plan	9
2.4.2 Modifications To The Project Plan	9
2.4.3 Deletions From The Project Plan	9
3 Design	9
3.1 Previous Work And Literature	9
3.2 Design Thinking	11
3.3 Proposed Design	13
3.4 Technology Considerations	14
3.5 Development Process	14
3.6 Design Plan	14
3.6.1 Simulation Plan	14

3.6.2 Nanogrid Experiments	15
4 Implementation	16
4.1 Inverter topology	16
4.1.1 Grid-Following Inverter	16
4.1.1.1 Bridge	16
4.1.1.2 Filter	17
4.1.1.3 Inverter Control	19
4.1.1.3.1 PLL & Measurements	19
4.1.1.3.2 VDC Regulator	21
4.1.1.3.3 Current Regulator	22
4.1.1.3.4 Reference Signal Generation	22
4.1.2 Grid forming Inverter:	23
4.2 Generation Sources	24
4.2.1 Solar PV subsystem	24
4.2.1.1 PV array	25
4.2.1.2 Maximum Power Point Tracking (MPPT)	27
4.2.1.3 Tracking accuracy	28
4.2.1.4 DC/DC boost converter	29
4.2.2 Wind Energy	30
4.2.2.1 Overview	30
4.2.2.1.1 Wind Turbine	30
4.2.2.1.1.1 Wind Energy Conversion	32
4.2.2.1.1.2 Permanent Magnet Synchronous Generator (PMSG)	33
4.2.2.1.2 Rectifier	33
4.2.3 Hydrogen Energy	34
4.2.3.1 Fuel Cell Stacks	34
4.2.3.2 Flow rate regulation system	35
4.2.3.3 Boost converter	36

4.2.3.4 Hydrogen tank + electrolyzer	37
4.2.4 Battery simulation	37
4.2.4.1 Battery model	37
4.2.4.2 Buck/Boost converter	38
5 Testing	39
5.1 Microgrid Testing/Simulation	39
5.1.1 PV array model plots	42
5.1.2 Wind Turbines model plots	42
5.1.3 Hydrogen Fuel Cells model plots	43
5.2 Nanogrid Testing	43
6 Closing Material	48
6.1 Conclusion	48
6.2 References	49
Appendix I - Operation Manual	50
Nanogrid	50
Simulation	52
Appendix II - Initial design	53

List of figures/tables/symbols/definitions

Fig. 1: Design sketch for Microgrid.	13
Fig. 2: High Level Diagram of Nano-Grid Design.	15
Fig. 3: Single phase bridge.	17
Fig. 4: Filter topology.	18
Fig. 5: Inverter control	19
Fig. 6: PLL & measurements	20
Fig. 7: Single-Phase dq transform (current)	20
Fig 8: How ABC, alpha-beta-zero, and d-q values are related	21
Fig. 9: VDC Controller	21
Fig. 10: Current Regulator	22
Fig. 11: Reference Signal Generation	23

Fig. 12: Grid forming inverter dq transformation block	24
Fig. 13: System Design Overview	24
Fig. 14: I-V curve (varying irradiances)	26
Fig. 15: P-V curve	26
Fig. 16: MPPT control overview	27
Fig. 17: MPPT algorithm for PV array	28
Fig. 18: MPPT tracking accuracy	29
Fig. 19: DC/DC boost converter topology	29
Fig. 20: Diagram of Wind Subsystem	30
Fig. 21: Diagram of Wind Turbine Model	30
Fig. 22: Performance characteristics of the Simscape Wind Turbine	32
Fig. 23: Rectifier topology	33
Fig. 24: System overview: Hydrogen fuel cell stacks + electrolyzer + fuel tank	34
Fig. 25: Flow rate regulation system	35
Fig. 26. Fuel characteristic, utilization, efficiency, and fuel consumption	36
Fig. 27: Power, Current, Voltage out of Boost Converter	37
Fig. 28: Bidirectional DC/DC converter with control	38
Fig. 29: RMS value of the output voltage of the system	40
Fig. 30: Real and Reactive power of the model	41
Fig. 31: Real and Reactive power plots for PV arrays	42
Fig. 32: Wind turbine output current	42
Fig. 33: Real and Reactive power output of the hydrogen fuel cell stack	43
Fig. 34: Solar Panel and Battery Testing	45
Fig. 35: Stack voltage as a function of current density	47
Fig. 36: Stack power as a function of current	48
Table 1: Nano-Grid Component List	16
Table 2: Filter components value	18
Table 3: Solar panel module characteristic	25
Table 4: Wind Turbine model characteristics	31
Table 5: Conversions between SI and power units	32
Table 6: Hydrogen fuel cell stack specifications	35
Table 7: Battery model parameters	38
Table 8: Event for interconnected simulation	40
Table 9: Solar panel and battery performance tests	46

1 Introduction

1.1 ACKNOWLEDGEMENT

Special thanks to Dr. Anne Kimber and Dr. Nick David, for their mentoring and assistance. Regards to Dr. Wenzhen Li and his graduate student Hengzhou Liu for aiding us in the conduction of performance testing on our hydrogen fuel cell.

1.2 PROBLEM AND PROJECT STATEMENT

1.2.1 Problem Statement

An electrical outage caused by an event such as a thunderstorm or blizzard can have devastating effects on our ability to communicate. These impacts can be seen in the loss of power to communications networks, which can inhibit businesses and disable critical communication between emergency crews. The resultant inability to inform residents within the impacted area is severely inhibited. Such impacts can be both monetarily costly and deadly. The susceptibility of communications systems to severe weather events is largely due to lack of energy resilience. As defined by the National Renewable Energy Laboratory (NREL), an energy resilient site “can continue to power critical operations (including the water, transportation, and communication systems that depend on energy) during natural disasters or human-caused incidents and recover rapidly after any disruption.” [14]

1.2.2 Project Statement

In order to increase energy resilience of communications systems, we designed a mobile microgrid capable of powering communications hubs for an extended period of time. The power produced by the microgrid is generated entirely by renewable resources; which include photovoltaic (PV) arrays, wind turbines, and hydrogen fuel cells. Each subsystem of the microgrid was designed with MATLAB/SIMULINK. After integrating each aspect of the microgrid, we ran simulations to verify the capabilities of our design. In addition to the simulations, we conducted tests on components of a microgrid including a 100 W solar panel, 518 Wh battery, and a 30 W hydrogen fuel cell stack. For the rest of this paper, the physical testing of small-scale components will be referred to as nanogrid experiments.

1.3 OPERATIONAL ENVIRONMENT

The microgrid is designed to operate in Kossuth County, IA. The components can be stored inside of a shipping crate capable of being easily transported between locations. Most components will be protected from outside weather conditions, but some, such as wind turbines and solar PV array, may be exposed. Those components that need to be capable of withstanding Iowa weather include, but are not limited to wind, snow, ice, and heat.

1.4 REQUIREMENTS

- The microgrid must be able to supply a 12 kW constant load
- The microgrid must output AC 120 V/60 Hz.
- The microgrid must be built entirely from components available on the market.
- The microgrid must be transportable within a 20' shipping container.

1.5 INTENDED USERS AND USES

The microgrid will be operated by utility companies providing communication infrastructure. The intended target for our designs will be to power a communications hub in northern Iowa that provides internet access to the area. The primary use for the simulation is to provide high resolution data of system behavior during transient events.

1.6 ASSUMPTIONS AND LIMITATIONS

1.6.1 Assumptions:

- The product will be used in North Central Iowa (Kossuth county).
- The shipping crate will be stationary on a reasonably level surface while it is being used.
- The load required will be at most a 12 kW constant value

1.6.2 Limitations:

- Produce 120V/60 Hz AC voltage, 12 kW power output.
- The design should not exceed the volume of a 20' shipping container in its transportation configuration

2 Project Plan

2.1 TASK DECOMPOSITION

1. Simulate the microgrid using SIMULINK.
 - a. Simulate the individual components
 - i. Hydrogen fuel cell system
 - ii. Photovoltaic (PV) array
 - iii. Wind turbine
 - iv. Battery with Bi-directional grid-forming inverter
 - v. Grid-following inverter
 - b. Pair the fuel cell system, wind turbine, and PV array with grid-following inverters. Perform simulations on these systems.
 - c. Integrate all systems into one simulation.
2. Test nanogrid components.
 - a. PV array
 - b. Battery/Inverter

c. Hydrogen Fuel Cell

2.2 OTHER RESOURCE REQUIREMENTS

This simulation software we used was MatLab/Simulink.

For testing and measurement we used:

- Multimeters and probes to measure and test the nanogrid under different scenarios.
- Compressed Hydrogen, Argon, and Nitrogen gas.

2.3 FINANCIAL REQUIREMENTS

For this project, we acquired \$5,000 from EPRI GridEd to build a nanogrid design of our simulation as a prototype. The team will present the results to an EPRI panel by October 2021.

2.4 PROJECT PLAN CHANGES

Between the end of EE 491 and the end of EE 492 the following changes were made to the project plan.

2.4.1 Additions To The Project Plan

The original project plan called for testing of the hydrogen fuel cell to be performed solely by the senior design team. After consideration of the testing equipment and expertise needed, the senior design team sought the assistance of Dr. Wenzhen Li and the use of his laboratory in order to test the hydrogen fuel cell.

2.4.2 Modifications To The Project Plan

At the end of EE 491, we planned to build a nanogrid using a small-scale version of each component used in the simulation. Due to budget and time limitations, it was decided to forego testing of a wind turbine and grid-following inverters, and conduct nanogrid experiments only on a PV Array, Battery/Inverter, and Hydrogen Fuel Cell as stated in figure 2.

2.4.3 Deletions From The Project Plan

It was initially intended to perform an economic analysis and a sustainability analysis of our designed microgrid. At the EE 491 end of semester presentation, the panel advised us to remove the conduction of these analyses from our project, due to the intensive workload needed to complete the project. For similar reasons, we did not perform tests on an already existing microgrid, and focused solely on the nanogrid experiments and simulations.

3 Design

3.1 PREVIOUS WORK AND LITERATURE

While microgrids are a more recent technology, a substantial amount of groundwork has been laid. In the paper “MICROGRID: A Review”, the authors defined microgrid as a single controlled unit that often consisted of generators, energy storage and load controllers as well as interfaces like inverters^[1]. The paper also lays out the importance of MGs in today’s power grid, such as the ability

to maintain power supply during natural disasters and improved reliability and quality of power received by the customers. The textbook, “Distributed Energy Resources in Microgrids: Integration, Challenges and Optimization” offers the history of microgrid (MG) research and development, common configurations of microgrids, and advantages and disadvantages of various components and configurations.^[3]

Some advantages of previous microgrids include well established combinations of the various energy generation and storage systems, existing technology designed to connect and manage energy generation and storage systems, and thoroughly developed simulations for individual components. The main shortcomings are that microgrids and more generally distributed energy resources are not as widely accepted. They typically have high upfront costs, and the large scale infrastructure has not been as fully developed as more traditional centralized forms of energy delivery.^{[1][3][4]} The lack of appearance of mobile microgrids in research papers and textbooks indicates that this is a novel adaptation of the newly established microgrids.

AC based microgrids have the advantage of being able to connect to most pre-existing grids. Additionally, many of the components within an AC system are well established and therefore generally less expensive and more reliable. Drawbacks of AC systems are lower efficiency due to conversion losses, integration with renewable technologies, and lower overall stability due to the larger number of necessary devices, conversion levels, and frequency matching requirements when synchronizing.^[1] DC microgrids require less conversion steps and components. Lack of need for costly conversion mechanisms leads the DC microgrids to be cheaper than AC microgrids when using entirely new components, but can be more costly if AC microgrids use existing distributed energy resources. DC microgrids also pose the advantage of increased efficiency. The DC microgrid disadvantages include need for bidirectional converters to connect to the main grid, and lack of standards for systems.^[1]

A common trend in microgrid design is to have systems that are separated by AC and DC buses. These microgrids offer the ability to interface with the main grid or existing AC systems. This allows for increased stability of the microgrid, enabling the system to use the main grid as a battery and charge storage devices at times when the microgrid is not needed to supply power. The AC and DC buses can connect directly to AC and DC loads. Microgrids that use both AC and DC buses will often use a bi-directional interlinking converter (BIC) to allow power flow between the two buses. It is especially important to use a synchronous switching control strategy, so that when interconnecting the two buses there is no instantaneous current due to a voltage and phase difference between the two sides of the connection point.^{[1][5]}

IEEE Standards for Microgrid Controllers^[6] defines a set of guidelines for building microgrid control systems. This standard allows for different controllers and components to operate cohesively and platform-independent. One of the most important management systems of microgrids is the microgrid energy management system (MEMS). According to the standard, the control functions enable the microgrid to operate autonomously or grid connected, as well as connect and disconnect to the grid smoothly. Control systems play an important role in microgrids, and are often technically challenging.

Microgrids have been implemented across the globe to play various roles in connected distributed energy resources. Some provide fail safes for grid power loss and increase stability in power supply. Other microgrids act purely in island mode to allow for power connected off-grid living. Some microgrid systems supply communities with energy distribution for locally generated renewable energy. A commonality between various roles of microgrids are the types of energy generation sources typically used. The most common generation sources currently implemented in microgrids are PV panels, diesel generators, and wind turbines. Some less common generation methods include hydro-electricity and hydrogen fuel cells. Lithium batteries are the most common energy storage method whereas methods like flywheel storage, hydrogen synthesis and pumped hydro are less common storage methods.^{[1][3][4][8]}

Some of the most successful case studies of microgrids include a hybrid combination of solar/wind and diesel generation. The system referenced by "Hybrid PV - Wind Driven Generator Supplying AC/DC Microgrid for Rural Electrification" utilizes both solar and wind generation with storage capabilities in addition to a standby backup diesel generator. Both solar and wind have intermittency problems where enough power is not generated when it's desired. The battery storage capabilities allow energy to be stored when generation is at its maximum, then power can be delivered from the batteries. The diesel generator acts as a backup source to provide power when the batteries are charging; this allows for constant power flow at any given time. The hybrid system configuration is the most common due to its increased reliability and affordability.^[6]

3.2 DESIGN THINKING

To better understand the problem we are trying to solve, we first had to understand the client. We were provided some specifications directly from the client that are seen below:

1. Communication companies need a way to power their data hubs during power outages, so the ability to communicate remains intact. Output power ought to be at least 12 kW.
2. They need the power generation to be mobile, in order to minimize the number of generation modules required.
3. They need to use primarily green energy, to prevent carbon emissions.

With this in mind, our team conducted extensive research into the world of microgrids in order to obtain an understanding of the current state and inner workings of the technology. The aspects that we have given the most attention to are as follows: microgrid review literature, energy generation devices, energy storage devices, inverters, microgrid control systems, use cases, communications infrastructure electrical load data, and simulation tools.

The first aspect we need to decide is which type of generation we want in our design. To solve this problem, we consult previous use cases as well as Dr. Kimber and Dr. David to narrow down our sources. During our discussion, we found that hydrogen fuel cells are a promising technology for storage but haven't been implemented into microgrids. Dylan volunteered to look more into hydrogen technology and how to implement it into our projects. After further discussion, we came to a conclusion with 3 generations type: solar panels, wind turbines for their popularity in microgrids and hydrogen fuel cells to test out their capability.

The second problem came when we had to decide whether to design a DC microgrid or an AC microgrid. A DC microgrid has the advantages of being simple and certainly easier to control because we don't have to worry about things like frequency and reactive power. However, an AC microgrid is chosen in our project simply because the majority of electrical appliances in our daily life nowadays run on AC current, so it makes sense to assume that the targeted communication hub runs on AC power. Finally, after the discussion, we came to a conclusion that the designs should always output 120V/60 Hz AC voltage and satisfy a 12 kW as mentioned earlier.

These three defined needs combined with the generation sources mentioned in section 3.1 led to the proposed design of the green mobile microgrid design. Some of the other design ideas, along with the reasons why they were not chosen, are listed below.

- Using a thermoelectric (seebeck) generator. This option, while intriguing, is simply not as efficient as using PV. ^[9]
- Using flow batteries rather than regular batteries. Flow batteries have a low energy density, are heavy, and expensive (\$257-390)/kWh Levelized Cost of Storage Wholesale [15]

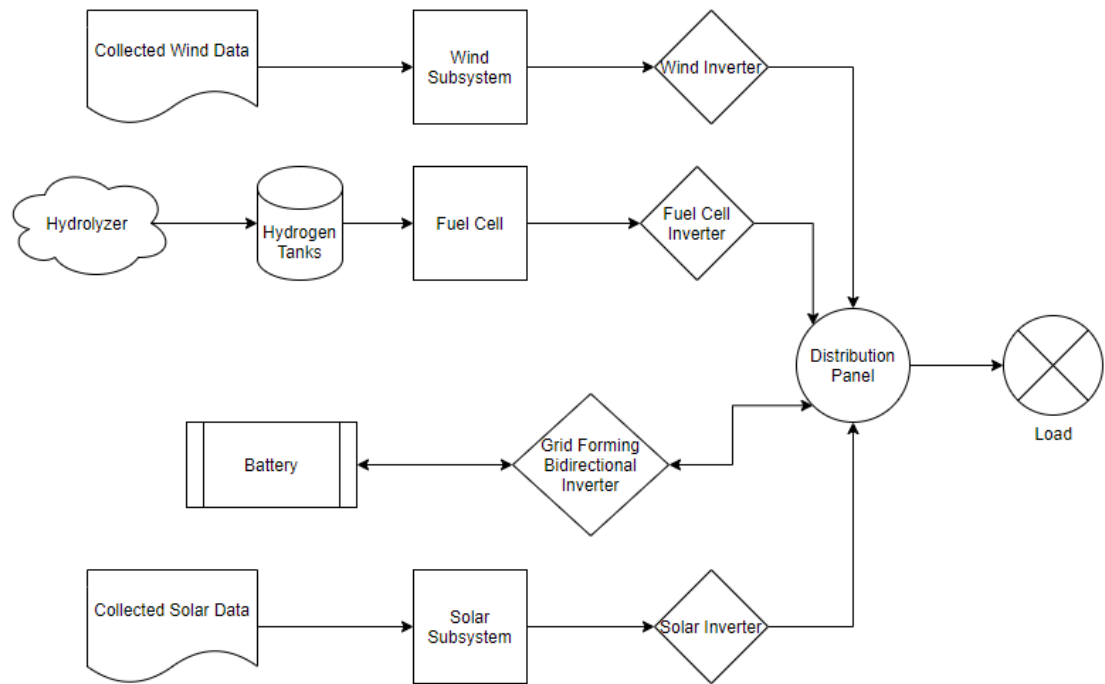


Fig. 1: Design sketch for Microgrid.

3.3 PROPOSED DESIGN

The microgrid we designed and simulated is an environmentally sustainable microgrid. The generation subsystem of this microgrid includes a wind turbine, hydrogen fuel cells, and PV panels. The storage subsystem consists of lithium ion batteries, hydrogen electrolyzer, and hydrogen storage tank. Inverters connect the storage and generation systems to a distribution panel, which then feeds to the load. The wind turbine is a horizontal axis wind turbine with a 23 m tower. The output of the wind turbine is a three-phase AC voltage. The electrical output is routed to an AC/DC rectifier which will feed into a single-phase inverter. The output of the inverter is routed to the distribution panel.

The PV subsystem outputs a DC voltage. The PV subsystem has a Maximum Power Point Tracking (MPPT) embedded into it. The MPPT decides which voltage the PV outputs to achieve maximum power, and from there the DC voltage is inverted and AC power is fed into the distribution panel. The lithium-ion batteries are connected to the distribution panel via a bi-directional inverter. The batteries operate at 48 VDC.

The hydrogen electrolyzer takes water as an input, and outputs hydrogen and oxygen. The hydrogen is directed to and stored in hydrogen tanks. A check valve is used to prevent backflow from the hydrogen tanks to the electrolyzer. The tanks, through a valve, direct hydrogen to the hydrogen fuel

cells. The hydrogen fuel cells, when needed, produce electricity and output water as a bi-product. The water is directed back to the hydrogen electrolyzer.

The components mentioned above were implemented in Simulink using building blocks from Simscape library under the Specialized Power System tab. From these blocks, one can use topology of the components and their parameters to simulate the behaviours of these components and interconnect them into a microgrid system.

3.4 TECHNOLOGY CONSIDERATIONS

The extent of existing power and electrical systems and components in Simulink is quite high through Simscape library. This allows for easy entry into the simulation of each individual device for our microgrid designs. However, there is a fairly steep learning curve in the control systems aspect of simulations. The control systems must be created specifically for each individual system and is one of the most important aspects of the simulation. Prebuilt systems offer lower learning curves, but can be quite costly in terms of money, and would not operate beyond outside of the niche software.

The ubiquity of Simulink's implementation allows for our systems to be run by any person that has MatLab and no additional licenses are required. Additionally, Simulink is a lower level software that allows for greater customization. We tailored our simulations to our needs to a much greater degree than we could have with other preexisting microgrid or energy system simulation softwares. Overall, using MatLab/Simulink allowed for greater simulation control and accessibility, at the cost of the need to overcome a steeper learning curve.

3.5 DEVELOPMENT PROCESS

Initially we followed a waterfall development process. This is due to the type of work that we were originally doing. A lot of research, documenting and grant writing does not lend itself very well to more iterative development processes. Once we began designing simulations and putting our prototype together, we relied on an agile-esque design process, where we implemented small components and tested that they function as intended. We then built up from those basic components and put things together into more complex systems.

3.6 DESIGN PLAN

3.6.1 Simulation Plan

The use case from section 1.5 gives us parameters in which to design our microgrid. Those parameters are as follows:

1. A binding constraint of 12kW constant load
 - a. need to have this much power provided at all times

- b. ideally always from a combination of stored energy and energy generation (not some consumable fuel)
2. A location, Kossuth county, used to obtain environmental data to be used as input for simulation model.

Our design plan contains six major steps:

1. Create simulations of each microgrid component
2. Run simulations and fine tune
3. Integrate generation components with grid-following inverters
4. Run simulations and fine tune
5. Integrate all components into final simulation
6. Have the results from integrated simulation advised by our advisors and adjust the model accordingly.

Requirements from section 1.4 will be met by our design plan as detailed below:

- The microgrid design will be able to provide a 12kW constant load
- The microgrid should supply AC 120V/60Hz
- The microgrid should be built entirely from components available on the market
- The microgrid must be transportable within a 20' shipping container

3.6.2 Nanogrid Experiments

The simulation parameters from the initial simulation in Simulink discussed in 3.3 will be adjusted to simulate a nanogrid. With a grant funded by GridEd, we purchased 100 W solar panels, 518 Wh battery and 30 W hydrogen fuel cell to build a nanogrid experiment. The focus of this prototype nanogrid is to show the integration of hydrogen fuel cells with known generation sources of microgrids like solar panels. The plan is to have the battery's inverter control the output voltage of the nanogrid.

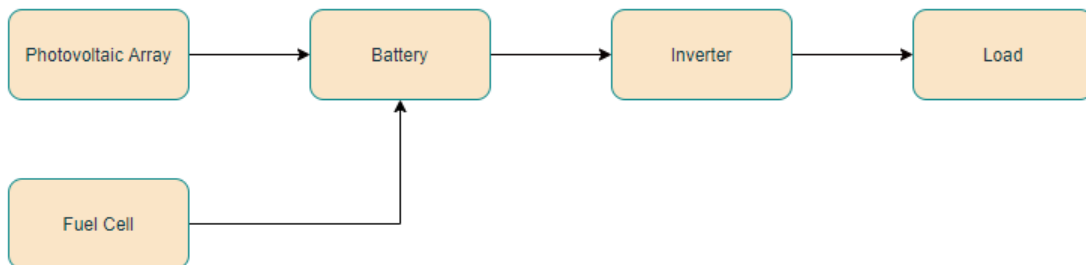


Fig. 2: High Level Diagram of Nano-Grid Design

Table 1: Nano-Grid Component List

Component	Price (\$)
30 W Hydrogen Fuel Cell	1,091
518Wh Lithium Battery	499
100W Solar Panel	299
Hydrogen Cylinder UHP 80 (70ft ³ ultra high purity H ₂).	100
Tubing, wiring, regulators provided by ISU via Dr. Wenzhen Li and ETG	N/A
Total	1989

In our nanogrid, the main source of generation will be solar panels and the fuel cell. The solar panels will be connected directly to the battery as there will be a MPPT device embedded in it. The built in inverter of the battery outputs AC voltage that will be connected to the load. The anode of the fuel cell uses a compressed composite gas of 70% Hydrogen and 30% Argon and the cathode uses ambient air. The output power from the fuel cell also acts as a DC input for the battery. Voltage and current sensors will determine the power output of each device.

4 Implementation

4.1 INVERTER TOPOLOGY

4.1.1 Grid-Following Inverter

The grid-following inverter is divided into three main sections: The diode bridge, filter, and control.

4.1.1.1 Bridge

Below is shown a single-phase IGBT-Diode bridge. For our purposes, a DC voltage is applied (shown on the left side of the image). A voltage signal (from the inverter control) is also applied to the transistor gates. The voltage is varied high to low to control the output of the diode bridge.

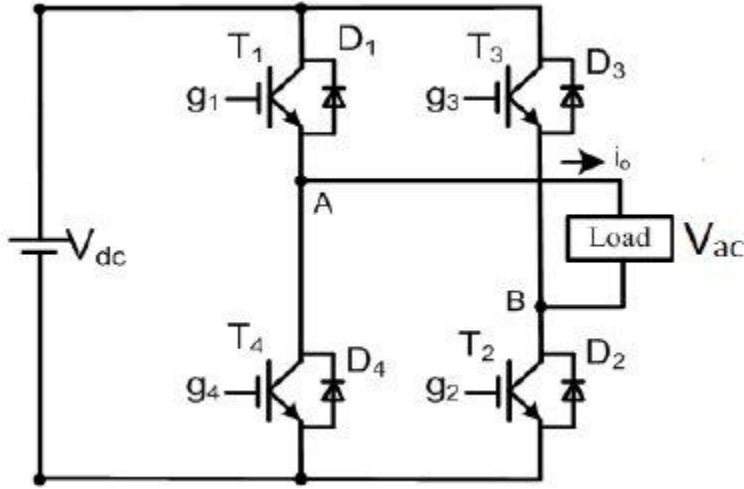


Fig. 3: Single phase bridge

4.1.1.2 Filter

The output of the bridge will be a high frequency (in our case this is 1090 Hz), dependent on the reference signal input at the transistor gates. A lowpass filter is used to remove the high-frequency signal components, leaving a signal of 60 Hz at the output. We used a fifth order lowpass filter with the component values outlined in the below table. The design process is as follows:

Step 2: Calculate the base impedance and capacitance, and design the capacitor size to be 5% of the base capacitance.

$$Z_b = \frac{V_{nom}^2}{P_b} \implies C_b = \frac{1}{2\pi f_b Z_b} \implies C_f = 0.05 C_b$$

Step 3: Design the inverter side inductors based on the allowed ripple of the rated current. Use 10% allowed ripple.

$$\Delta I_{Lmax} = 0.1 I_{max} = 0.1 \frac{P_b \sqrt{2}}{V_{nom}} \implies L_1 = L_3 = \frac{V_{dc}}{12 f_{sw} \Delta I_{Lmax}}$$

Step 4: Design the grid-side inductors based on the desired attenuation for the harmonic current generated by the inverter. Set $k_a=0.2$ in the simulation modeling.

$$L_2 = L_4 = \frac{\sqrt{1/k_a^2 + 1}}{2C_f (2\pi f_{sw})^2}$$

Step 5: Check if the resonant frequency of the filter meets the condition

$$10f_g \leq f_{res} = \frac{1}{2\pi} \sqrt{\frac{L_1 + L_2}{L_1 L_2 C_f}} \geq 0.5 f_{sw}$$

If the condition is not satisfied, jump back to Step 4 and reset the attenuation for new values of the grid-side inductors. Otherwise, continue the next step.

Step 5: Design the resistance that is in series with the capacitor to eliminate the gain spike, smooth the overall response, and rolling-off to -180° for high frequency, instead of -270° .

$$R_f = \frac{1}{3(2\pi f_{res}) C_f}$$

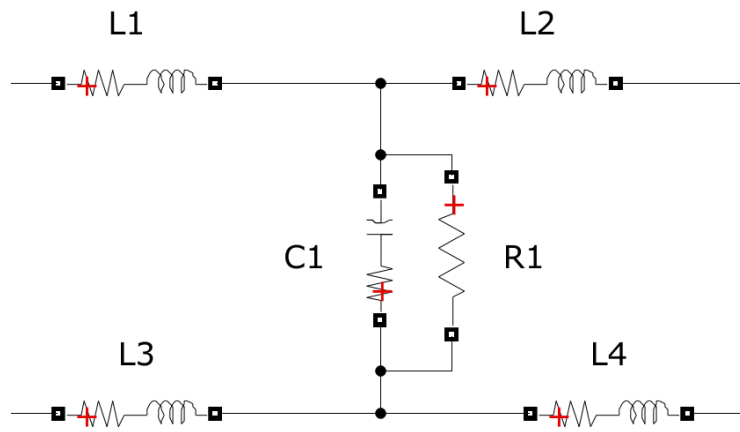


Fig. 4: Filter topology

The parameters are then modified as needed to achieve the desired feature of the output filter: sinusoid 60 Hz with 120 Vrms.

Table 2: Filter components value

Component	Values
Series Resistors	0.95 $\mu\Omega$
Series Inductors	3.9674 mH
Shunt Capacitor (load)	-131.25 VAR
Resistor in series with shunt capacitor (load)	2.625 W
Shunt Resistor (R1)	1000 Ohms

4.1.1.3 Inverter Control

The broad overview of the inverter control is this; The AC voltage, AC current, and DC voltage are measured. These values are used to find the DQ values of the voltage, current, radians (ωt) and the mean DC voltage value. In turn, a VDC regulator uses the VDC mean and a reference VDC value to create an Id reference value. A current regulator uses the input dq values for current and voltage, and the Id reference, to modify the Vd Vq values. The modified Vd Vq values are then used to generate a reference sinusoid that is input to a pulse-width-modulator, creating the reference signal that is applied to the gates of the transistors in the inverter bridge.

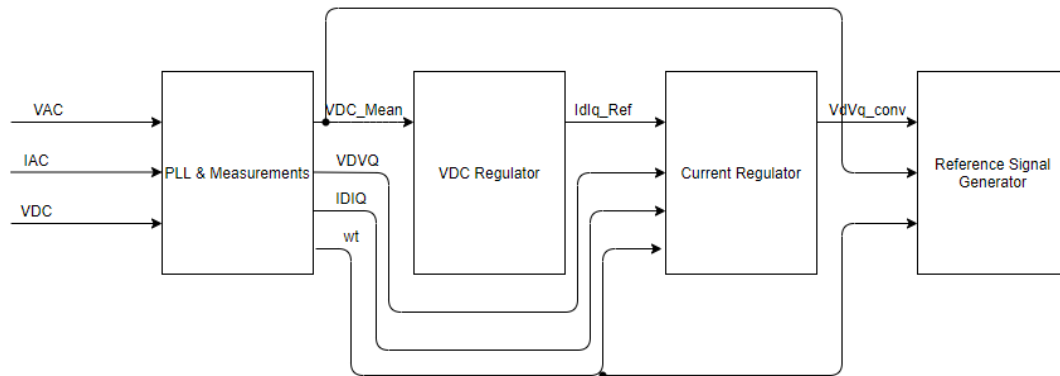


Fig. 5: Inverter control

4.1.1.3.1 PLL & Measurements

The AC voltage and current is first divided by base values in order to obtain the per-unit value. The base value of the voltage is $120V_{rms}$. The base current is dependent on the base power, which may vary from situation to situation. For our purposes, we defined the base power to be 15 MVA. The per-unit voltage is input to a phase-lock-loop (PLL) block, which outputs the frequency and phase angle ($\omega t = (\text{rad/s}) \cdot s = \text{rad}$). The frequency and angle are then used to obtain the Id, Iq, Vd, and Vq values. The Vd and Vq values are obtained using a Fourier transform to obtain the magnitude and angle of the signal, the real part of which is the Vd value, the imaginary part the Vq value. The process of obtaining the Id and Iq values is more complex, and has been provided its own subsystem. Figures seven and eight show these processes using flow charts.

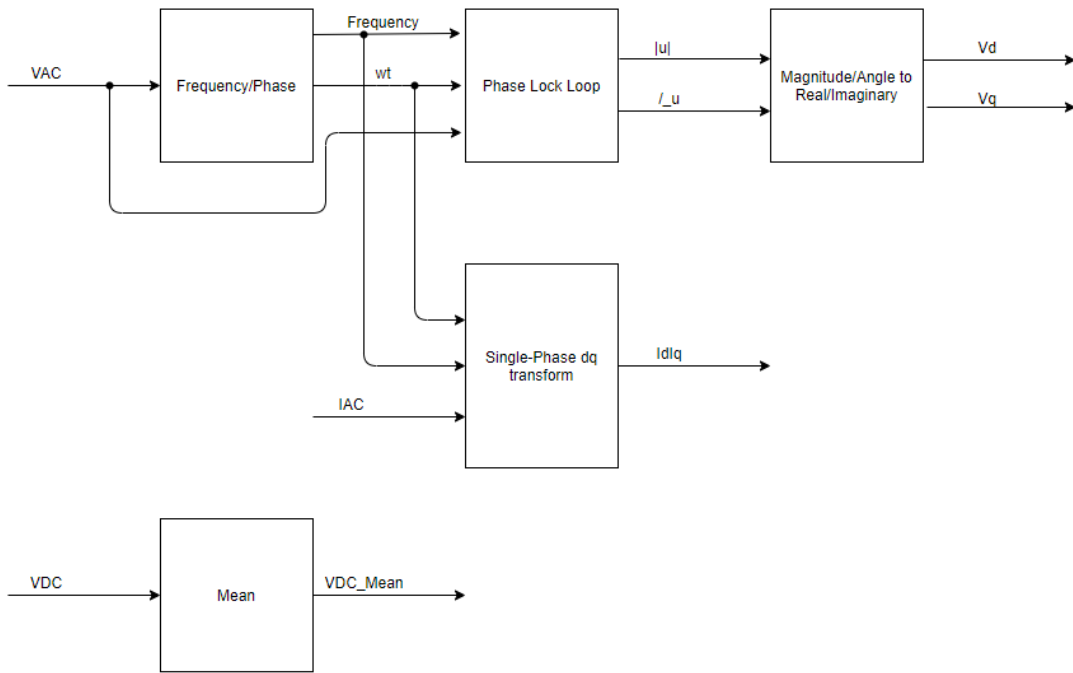


Fig. 6: PLL & measurements

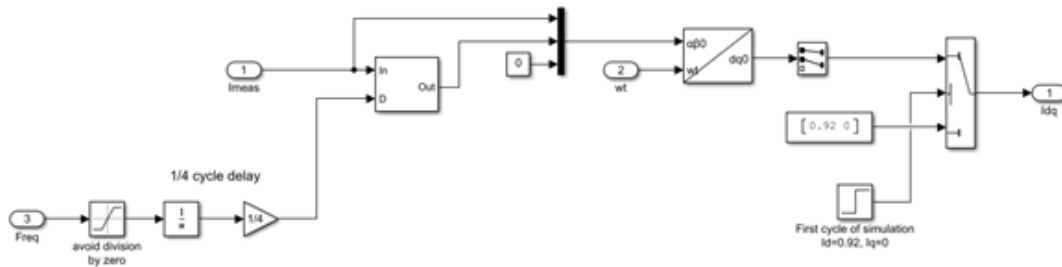


Fig. 7: Single-Phase dq transform (current)

The measured current value is delayed for a time period, and then the measured current values and delayed value are used as alpha and beta signals. From there, an alpha-beta-zero to d-q transform can occur. Fig. 9 can help with understanding how ABC, alpha-beta-zero, and d-q values are related.

Since this process requires at least one cycle (otherwise it would be difficult to obtain the delayed value), values of $I_d = 0.92$ and $I_q = 0$ are prematurely assigned.

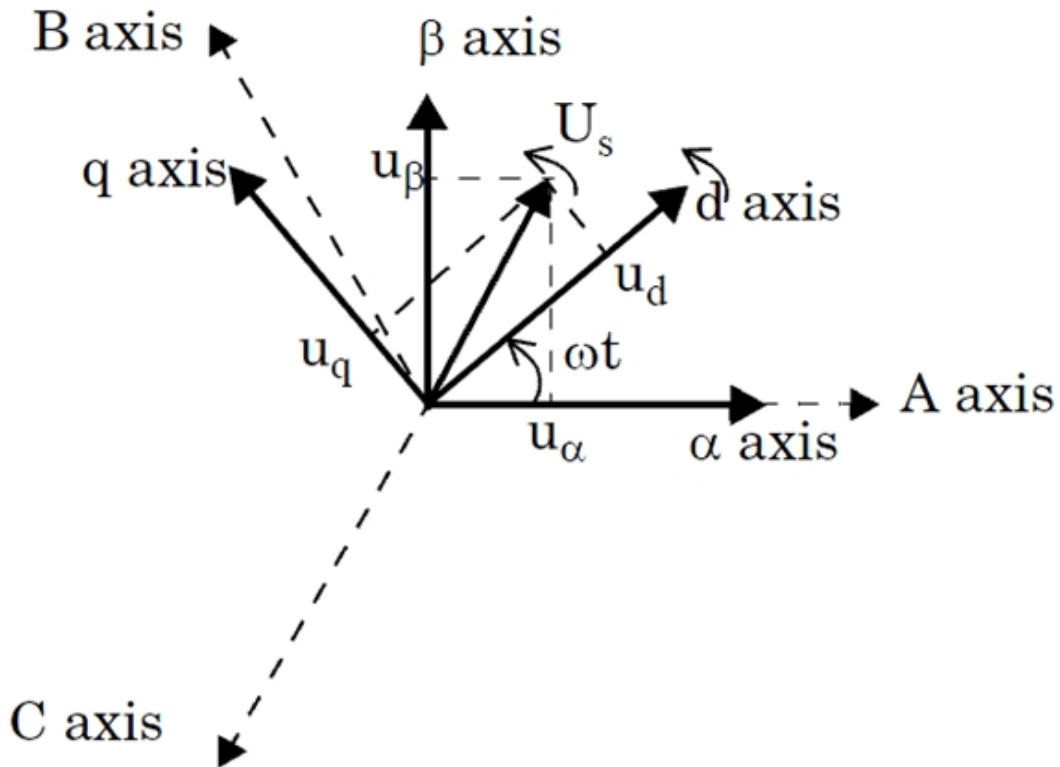


Fig. 8: How ABC, alpha-beta-zero, and d-q values are related [12]

The d-q reference frame can be useful for analyses of signals. The d-q reference frame is a rotating reference frame, which varies based on the phase angle ωt . As the frame rotates, the positions of the d and q axes remain fixed relative to ωt . This means that for a balanced three-phase signal, d and q remain constant regardless of the phase angle.

4.1.1.3.2 VDC Regulator

The mean VDC value is compared to a reference value, and divided by a nominal value to obtain a per-unit quantity. This value is then fed into a PI controller in order to obtain the I_{d_ref} value (see table below for input values). PI control values were chosen through an iterative process.

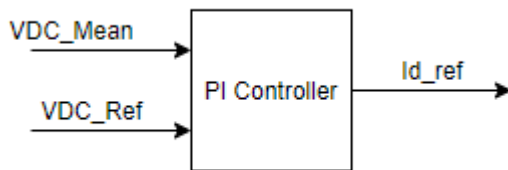


Fig. 9: VDC Controller

VDC Controller P = 35.09

VDC Controller I = 79.3876

$T_s \approx 5 \mu s$

$$\text{Transfer Function: } C(z) = P + \frac{I \times T_s \times (z+1)}{2(z-1)}$$

4.1.1.3.3 Current Regulator

The Id_ref value, as well as an Iq_ref value (defined as zero) are compared to the Id and Iq quantities which were identified in the PLL and measurements section of the control. The output is then fed into a PI controller. While this occurs, a mathematical equation is implemented (see below for details) involving Id, Iq, Vd, and Vq. A limit is imposed on the output when the function and PI output are summed. This new value will be used to create the reference signal input to the PWM. Similar to the VDC regulator, PI control values were chosen through iteration.

Current Regulator P = 5.1872

Current Regulator I = 51.1561

$$\text{Transfer Function } C(z) = P + \frac{I \times T_s \times (z+1)}{2(z-1)}$$

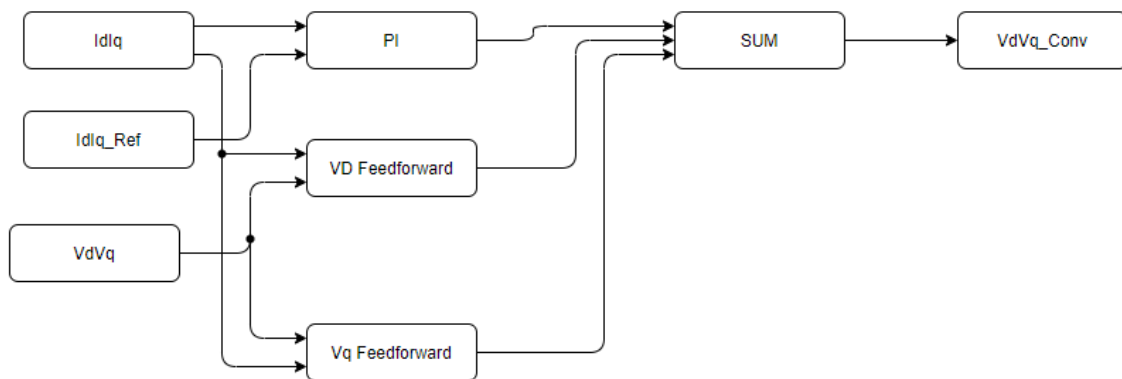


Fig. 10: Current Regulator

4.1.1.3.4 Reference Signal Generation

The VDC mean value is divided by the V_nom value (120 V) to obtain the per-unit value. It then modifies the magnitude of the converted Vd and Vq values, from which the magnitude and angle are obtained. The wt phase angle is added, along with the simulation control frequency and time to account for the signal delay. This sinusoidal waveform then becomes the reference signal for the PWM, which controls the switching function of the H-bridge.

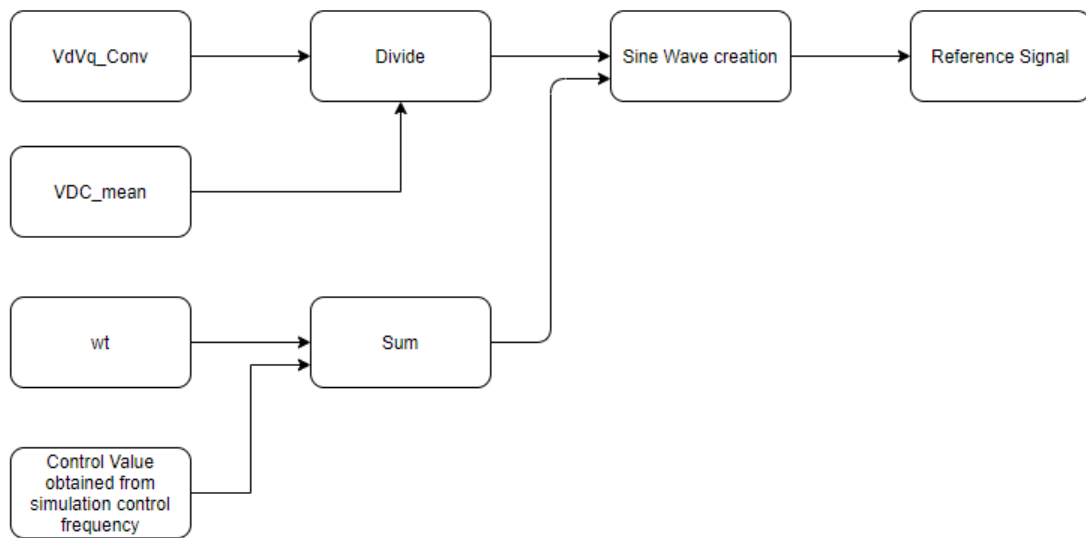


Fig. 11: Reference Signal Generation

4.1.2 Grid forming Inverter:

The Grid forming inverter has nearly the same control and bridge as the grid following inverter but has some key differences in its control mechanism. It utilizes the times in Simulink and multiply that with the desired frequency (60 Hz) and feeds that to the single phase dq transformation to make sure that the grid can be synchronized to 60 Hz.

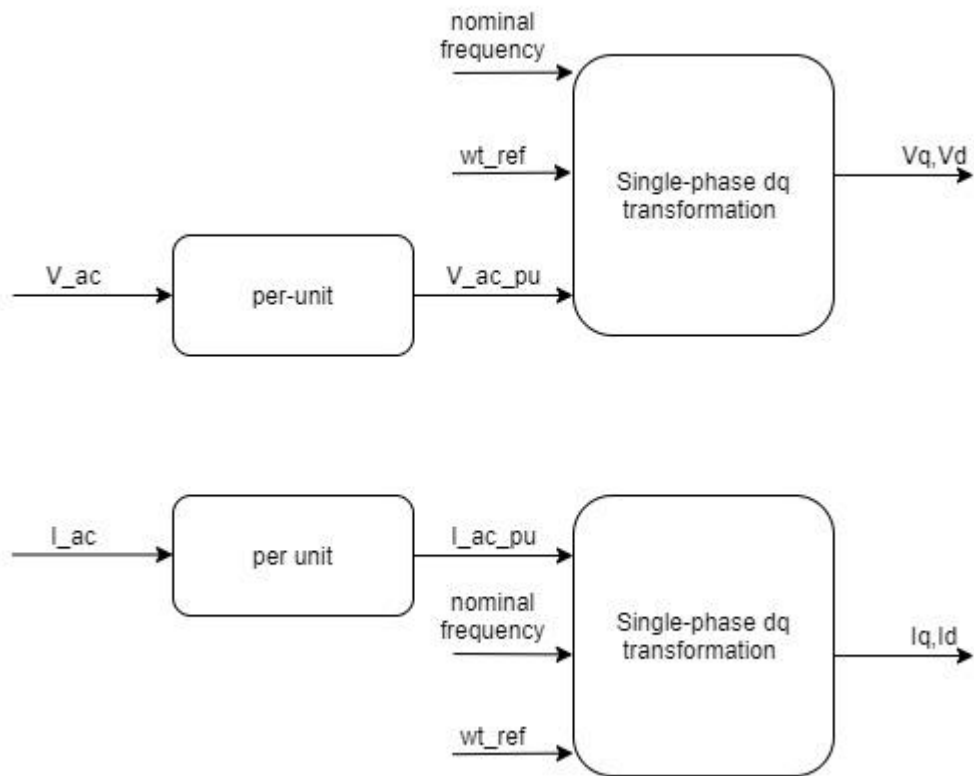


Fig. 12: Grid forming inverter dq transformation block

4.2 GENERATION SOURCES

4.2.1 Solar PV subsystem

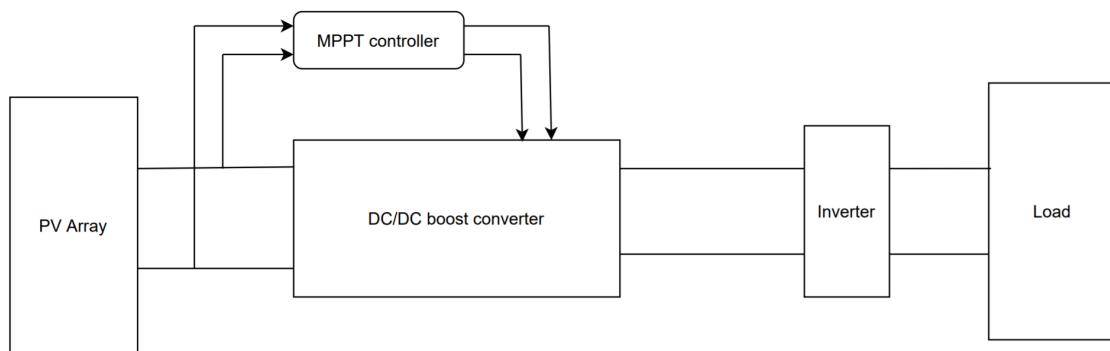


Fig. 13: System Design Overview

The diagram shown in Figure 13 shows the solar pv subsystem connected to the inverter and the load. The subsystem is composed of three major components, the solar pv array, Maximum Power Point Tracking (MPPT) controller, and the DC/DC boost converter.

4.2.1.1 PV array

For this component of the system we modelled a PV array. The array was composed of multiple strings of solar modules connected in parallel, with each string consisting of multiple modules connected in series in a grid structure. The total Maximum Power of the array $P_{MP, Array}$ can be calculated by the following equation.

$$P_{MP, Array} = P_{MP} (N_{series} N_{parallel})$$

For the purpose of simulating the performance of all the generation sources the PV array was sized at 6.1kW. As such with the module that was modelled the dimensions were 4 modules in series per string, and 5 parallel strings. These dimensions are subject to change depending on the required load, and the associated optimal sizing for that load.

To simulate this PV array we used the MATLAB/Simulink PV array block which allows the implementation of an array based on pre-selected commercially available PV modules. The inputs to this component are the related weather data, namely, Temperature ($^{\circ}\text{C}$), and Irradiance (W/m^2). The corresponding outputs are the voltage and current of the PV array V_{PV} and I_{PV} . The specific module that was selected for this simulation was the SunPower-SPR-305E-WHT-D, due to its relatively high efficiency and high P_{MP} . The characteristics for a single module are shown in table 3.

Table 3: Solar panel module characteristic

SunPower-SPR-305E-WHT-D specifications	
Maximum Power, P_{MP}	305 W
Voltage at Maximum power point, V_{mpp}	54.7 V
Current at Maximum power point, I_{mpp}	5.58A
Open circuit voltage, V_{oc}	64.2V
Short circuit current, I_{sc}	5.96A
Peak efficiency,	18.7%

To understand how the solar array performs under various conditions, we varied irradiance and plotted the Current vs Voltage and Power vs Voltage characteristics of the solar array as shown in figures 14 & 15

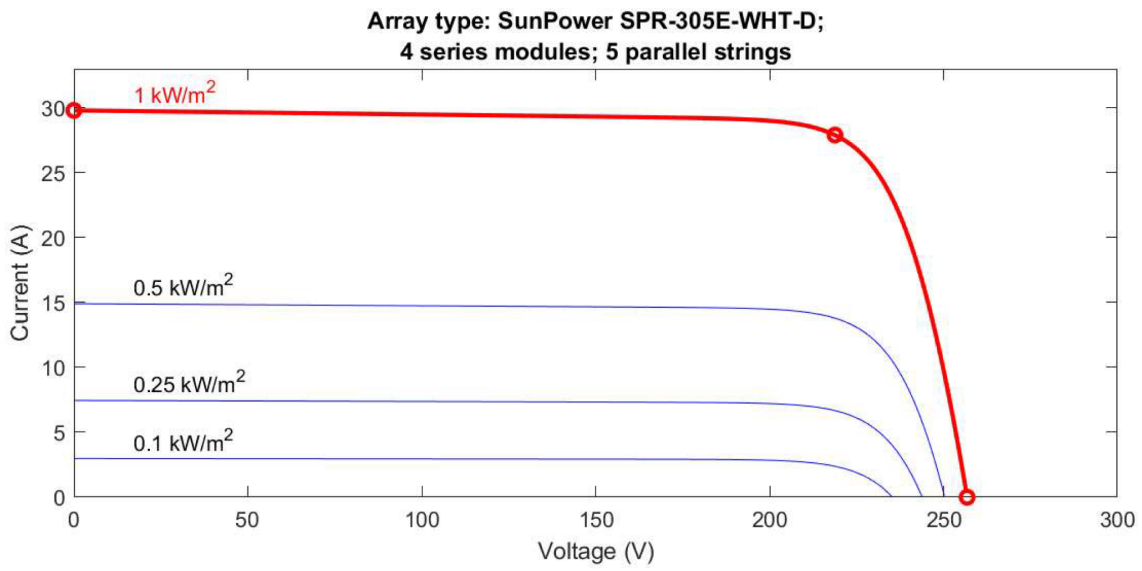


Fig. 14: I-V curve (varying irradiances)

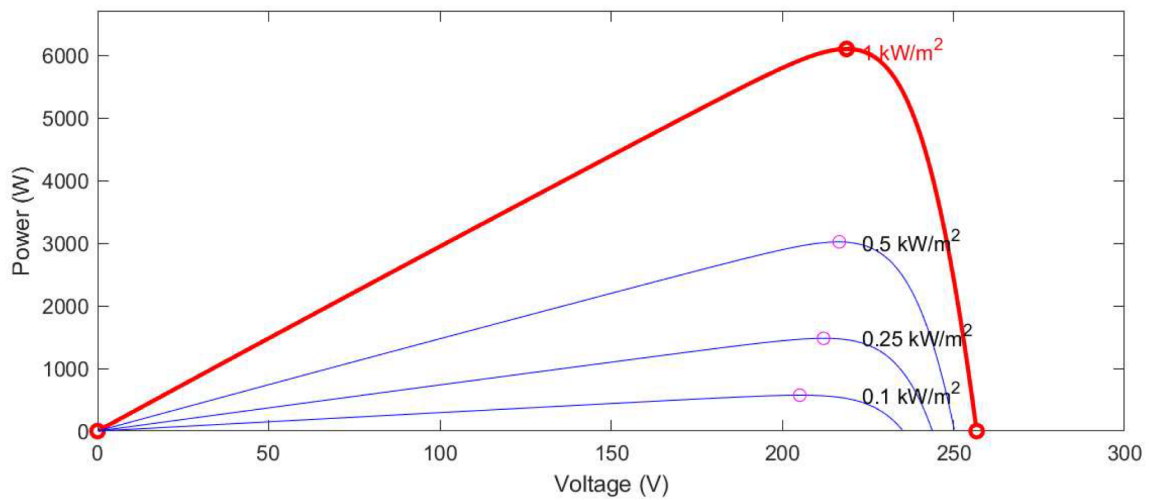


Fig. 15: P-V curve

4.2.1.2 Maximum Power Point Tracking (MPPT)

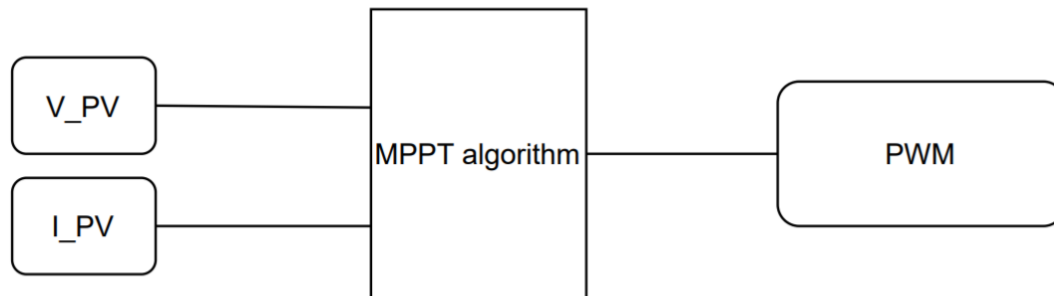


Fig. 16: MPPT control overview

The performance of a PV array system can be highly influenced by external environmental factors such as temperature, irradiance cloud cover etc. The variability of these factors is reflected in the performance of the array so to introduce uniformity to the systems performance a Maximum Power Point Tracking (MPPT) controller is necessary to regulate the power being delivered to the load. Throughout the literature there are various MPPT techniques, which can be categorized into classical methods (Perturbed & Observe and Incremental Conductance) and more advanced Artificial Intelligence techniques. For the purpose of this simulation P&O was used for its simplicity in implementation. Despite its simplicity it yields high tracking results. In addition to the fact that it is amongst the most commonly used methods [2].

This P&O algorithm works by taking in I-V values from the array and calculating power. It checks if MPP is reached by referencing previous power and voltage values on the Power vs Voltage plot and accordingly increments/decrements the duty cycle until MPP is reached for each input measurement. The steps of this algorithm are outlined in figure 17.

The MPPT controller outlined in figure 16 consists of an MPPT algorithm that determines the duty cycle that corresponds to the Maximum Power Point based on incoming current and voltage measurements. The duty cycle that is determined for each measurement is then fed into a PWM (Pulse Width Modulation) module with a switching frequency of 5000Hz which outputs a signal to the IGBT switch in the boost converter. The particular switching frequency was determined through experimentation.

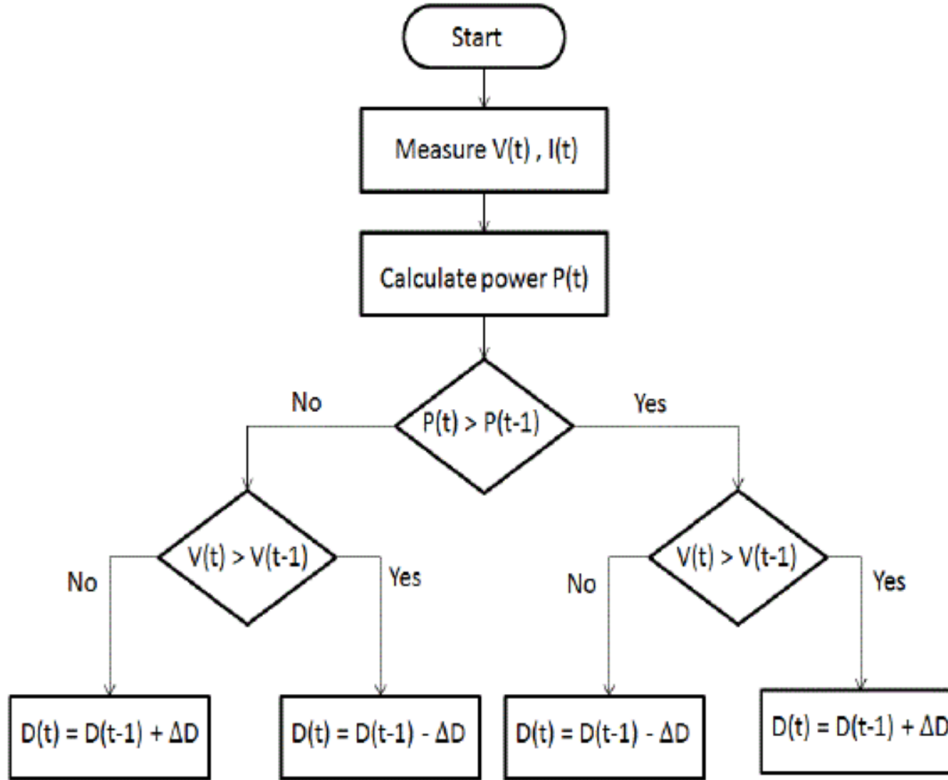


Fig. 17: MPPT algorithm for PV array

4.2.1.3 Tracking accuracy

In order to verify the tracking accuracy of the MPPT we varied the temperature and irradiance with a signal generator, and measured the corresponding PV array power output with the MPPT. Figure 18 shows the response of the MPPT controller to the changes in irradiance. Despite the simulated sudden changes in irradiance and temperature the tracking accuracy was in the range of 91-95%.

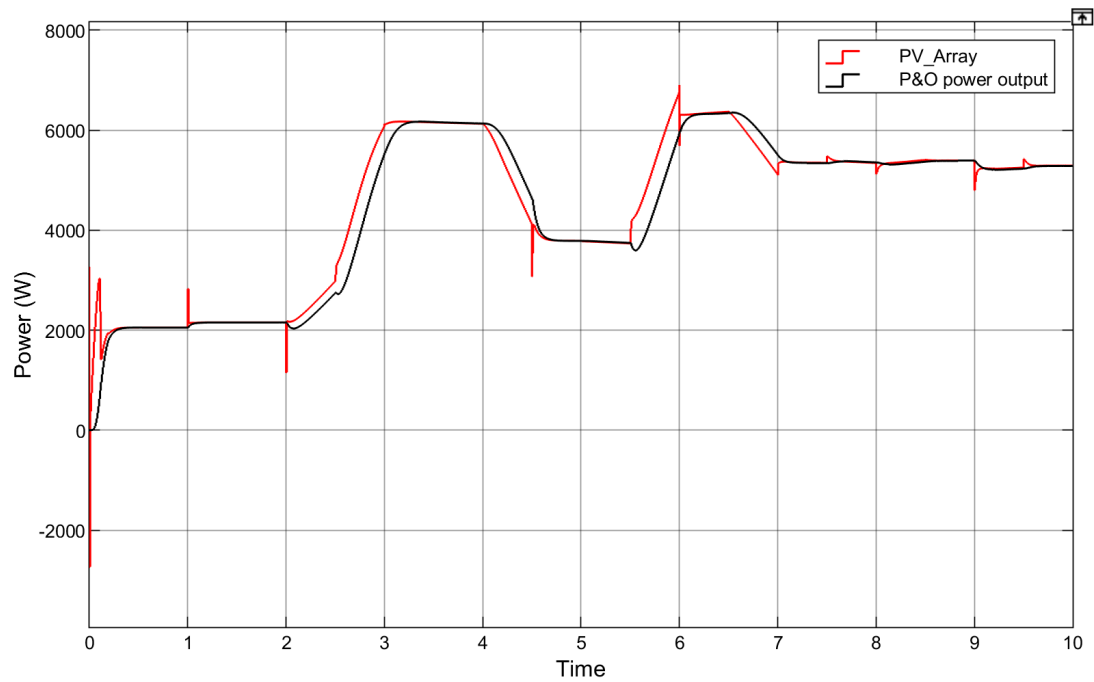


Fig. 18: MPPT tracking accuracy

4.2.1.4 DC/DC boost converter

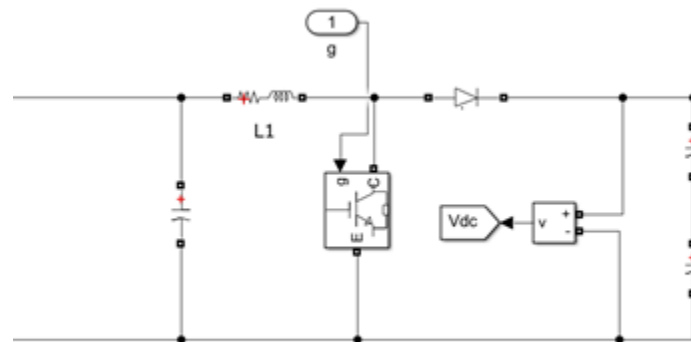


Fig. 19: DC/DC boost converter topology

The DC/DC boost converter is used to increase the DC voltage to avoid clipping the AC output of the grid inverter. The solar array acts as a DC voltage source to the boost converter. The output voltage of the solar array corresponds to the input voltage V_{in} of the boost converter. The converter is composed of capacitors/inductors and an IGBT switch. The MPPT controller determines the duty cycle, and the duty cycle determines the boosted voltage V_o . In our case the duty cycle would vary between 0.45-0.55.

$$\frac{V_o}{V_{in}} = \frac{1}{1-D}$$

4.2.2 Wind Energy

4.2.2.1 Overview

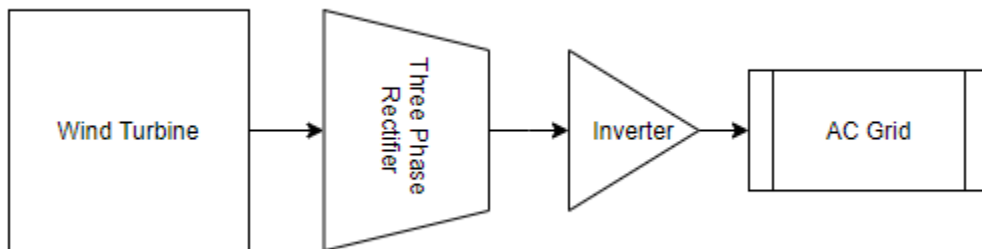


Fig. 20: Diagram of Wind Subsystem

The wind subsystem consists of a wind turbine, a three-phase rectifier, and one DC to AC grid following inverter. The Permanent Magnetic Synchronous Machine (PMSG) wind turbine will produce variable frequency three-phase AC power. To be synchronized with the one-phase AC grid, the turbine output must be rectified and then inverted to follow the grid side voltage. The DC to AC inverter utilizes a phase lock loop to follow and supply power to an existing AC grid.

4.2.2.1.1 Wind Turbine

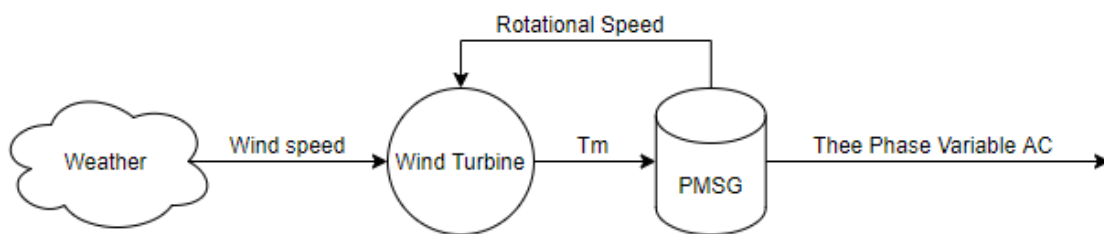


Fig. 21: Diagram of Wind Turbine Model

The wind turbine was modeled after an experimental turbine used in research at The Public University of Navarra in Spain^[10].

Table 4: Wind Turbine model characteristics

Wind Turbine characteristics	
Nominal power	4200 W
Wind speed for turn on	3.5 m/s
Wind speed for nominal power	12 m/s
Optimum power coefficient	0.316
Optimum tip speed ratio	8.63
Diameter of the rotor	4 m
Inertia	5 kg m ²
Height of the nacelle	23 m
Characteristic of the PMSG	
Nominal speed	600 rpm
Line voltage constant	475 V/krpm
Nominal current	11.6 A
Number of pole pairs	15 pairs
Stator equivalent resistance	.6 Ω
Stator equivalent inductance	4.9 mH

Various components of the model are designed for power units and some for actual, thus the following conversion must be done:

Table 5: Conversions between SI and power units

Generator speed: RPM to pu	Reduced multiplier
Generator Speed (pu) = $\frac{\text{Actual RPM}}{\text{Base RPM}} = \frac{\text{PMSG output}}{600 \text{ rpm}}$	1/600
Torque: pu to N*m	Reduced multiplier
$T_m (Nm) = T_m(pu) * \frac{VA}{\text{base speed(rad/s)}} = T_m(pu) * \frac{4666.6}{62.83 \text{ rad}}$	74.2745

4.2.2.1.1.1 Wind Energy Conversion

The power available in the wind can be calculated with the following equation, where P_m is the power in watts, C_p is the performance coefficient of the turbine, ρ is the air density (kg/m^3), A is the turbine swept area (m^2), v is the wind speed (m/s), λ is the tip ratio and β is the blade pitch angle (deg). For the turbine in this model, the blade pitch is a static 0 degrees.

$$P_m = C_p(\lambda, \beta) \frac{\rho A}{2} v^3 \quad [10]$$

The behaviour of the modeled turbine, using values in Table 5 is shown in the following chart.

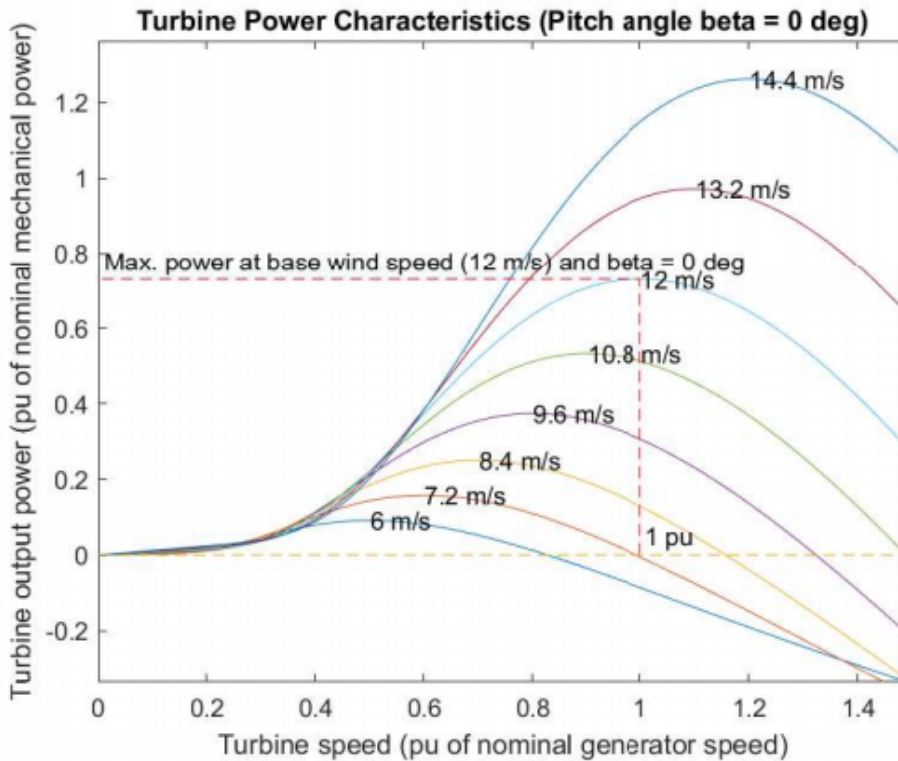


Fig. 22: Performance characteristics of the Simscape Wind Turbine

4.2.2.1.1.2 Permanent Magnet Synchronous Generator (PMSG)

A three phase PMSG was modeled to match the physical wind turbine characteristics stated in Table 4. The model is represented by the following equations:

$$\frac{d}{dt}i_d = \frac{1}{L_d}v_d - \frac{R}{L_d}i_d + \frac{L_q}{L_d}p\omega_m i_q$$

$$\frac{d}{dt}i_q = \frac{1}{L_q}v_q - \frac{R}{L_q}i_q + \frac{L_d}{L_q}p\omega_m i_d - \frac{\lambda p\omega_m}{L_q}$$

$$T_e = 1.5[\lambda i_q + (L_d - L_q)i_d i_q]$$

[13]

L_q, L_d are the q-axis and d-axis inductances, R is the resistance of the stator windings, i_q and i_d are the currents and v_q, v_d are the corresponding axis voltages. ω_m is the angular velocity of the rotor, λ is the flux amplitude induced between the stator phases and permanent magnets. T_e is the electromagnetic torque and p is the number of poles.

4.2.2.1.2 Rectifier

A simple three-phase diode bridge rectifier circuit, shown in Fig. 23, is used to convert the alternating current from the PMSG to DC for the inverter. Since the PMSG generates a three-phase AC signal with variable frequency, it must be converted to a steady one phase 60 Hz signal to operate with the grid. This is achieved by rectifying it to a steady DC voltage, and then again inverting it with a grid following inverter. Each diode is in parallel with a 1000 Ohm resistor and a 100 nF capacitor. These snubber components allow relief in the case of sharp spikes of voltage and current that occur when the wind turbine is connected or disconnected.

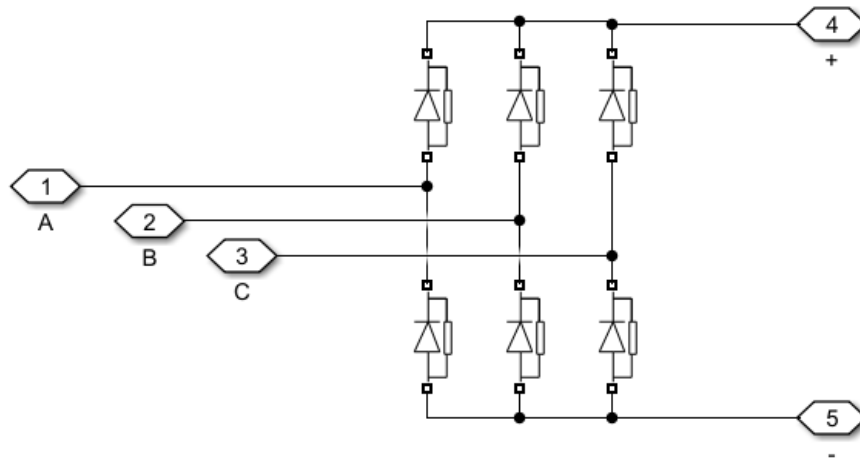


Fig. 23: Rectifier topology

4.2.3 Hydrogen Energy

The hydrogen energy system consists of two 6kW fuel cell stacks accompanied by a flow rate regulation system, a boost converter, a hydrogen tank and an electrolyzer. The fuel cell stacks are electrochemical models of the conversion from hydrogen and oxygen to water and electricity. The boost converter is an electrical performance model of boost conversion with constant duty cycle. The flow rate regulator is a control system based upon current output data. Both the hydrogen tank and the electrolyzer are mathematical abstractions to simulate hydrogen usage and production.

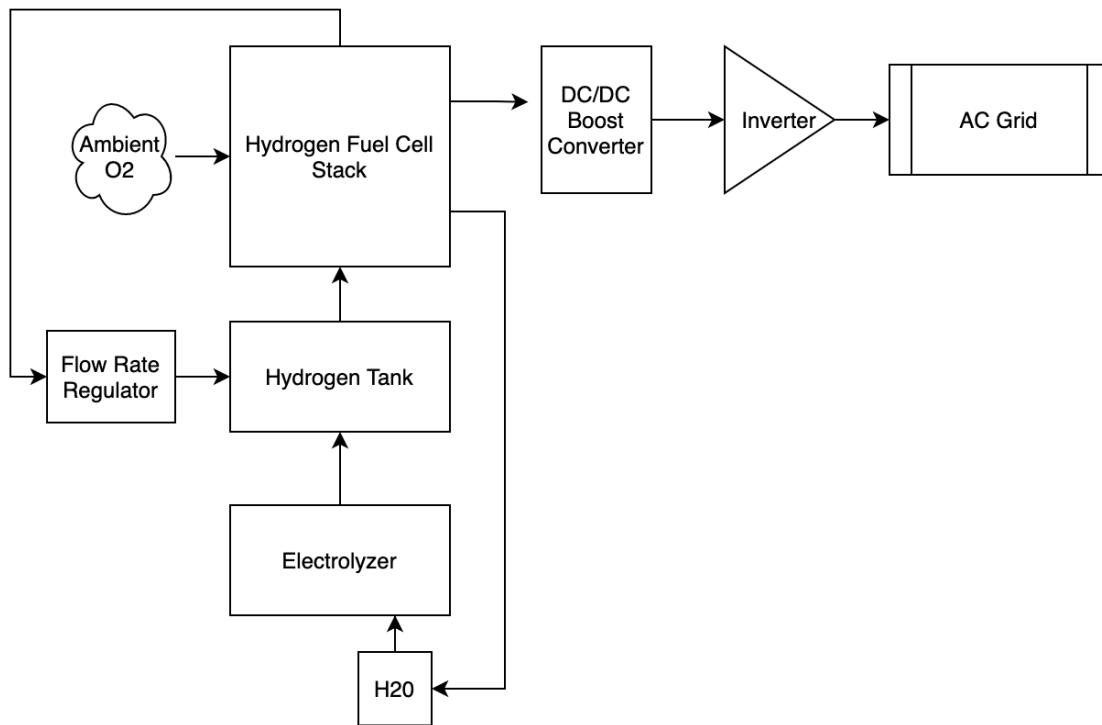


Fig. 24: System overview: Hydrogen fuel cell stacks + electrolyzer + fuel tank

4.2.3.1 Fuel Cell Stacks

The fuel cell stacks are each capable of producing 6kW of DC power. The production capability of each can be tuned to produce different amounts of energy through manipulation of device characteristics as shown in the figure below. These characteristics include; v_{oc} and i_A voltage values, nominal operating V and I, maximum operation V and I, number of cells in the stack, nominal efficiency of the stack, operating temperature, nominal air flow rate, nominal pressure, and nominal composition of hydrogen and oxygen. The fuel cell stacks are connected in series to create an output power of 12 kW. Situations in which solar and wind generation are sufficient enough to power at minimum half of the load, one of the cells can be disconnected to reduce power production to 6kW. If solar and wind are fully capable of supplying the load, the both fuel cells can be turned off. A combined power of 12kW was chosen so that the fuel cells can produce all of the power that is required to supply the load in the case that solar, wind, and battery power are insufficient. In this way, the fuel cells act as a backup generator. The fuel cell stacks take a flow rate data value as an input and output $V_{dc}(+)$ and $V_{dc}(-)$ at the respectively labeled (+) and (-) terminals. The fuel cells also output voltage, current, stack efficiency, stack consumption, and fuel utilization data values. The fuel cells can be modified to take inputs of fuel composition, oxidant composition, air flow rate, system temperature, fuel supply pressure, and air supply pressure. The

overall energy resilience of the microgrid is increased as a result of the constant power production ability of the fuel cell.

Table 6: Hydrogen fuel cell stack specifications

Hydrogen fuel cell stack specifications	
Voltage at 0 A and 1 A	65 V, 63 V
Nominal operating point I and V	133.3 A, 45 V
Maximum operating point I and V	225 A, 37 V
Number of cells	65
Nominal stack efficiency	55%
Operating temperature (Celsius)	30 C
Nominal air flow rate (lpm)	300 lpm
Nominal supply pressure of fuel and air	1.5 bar, 1 bar
Nominal composition % of H ₂ , O ₂ , H ₂ O	99.95, 21, 1

4.2.3.2 Flow rate regulation system

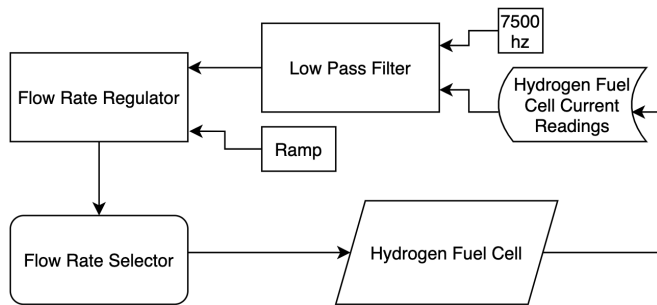


Fig. 25: Flow rate regulation system

The flow rate regulation system detects whether the current is moving towards or away from the optimal current and adjusts the flow rate accordingly. As the current density per area of fuel cell catalyst membranes increase, the power output will increase. This occurs until a saturation point, in which the mass transport can increase no further. After this point, the voltage will decrease at a rate that overwhelms the current increase and the power will decrease. A low pass filter is used to prevent rapid changes to current impact the flow rate. A ramp function is used to simulate gradually increasing the flow rate out of the valves of the hydrogen tanks.

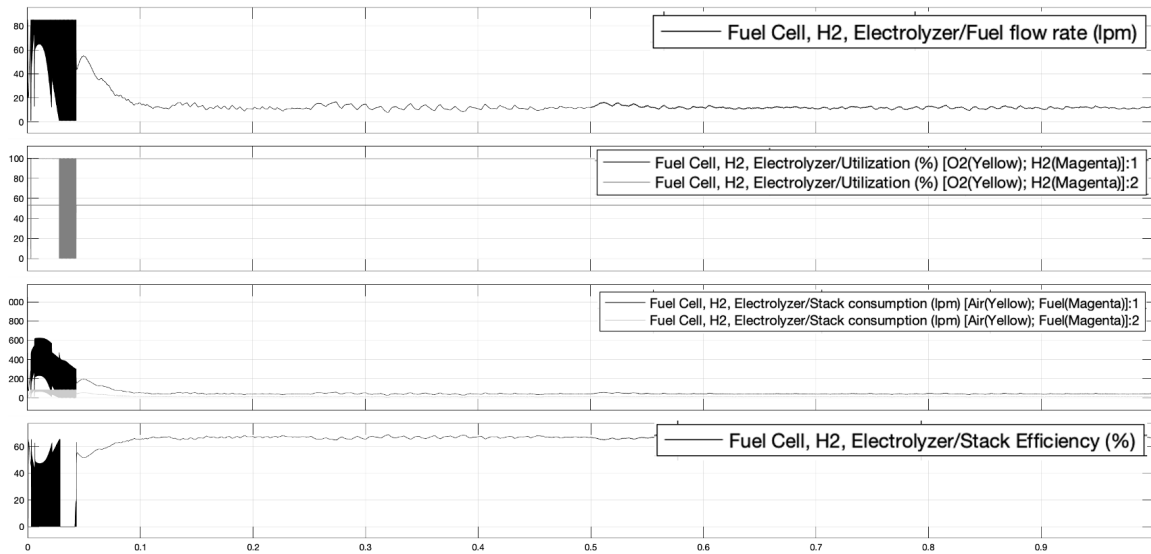


Fig. 26. Fuel characteristics: fuel flow rate, utilization, efficiency, and fuel consumption

The behavior of the fuel characteristics varies rapidly during the transient state of operation of the fuel cell stacks (the first ~0.04 seconds). The transience of the flow rates can be linked to the transient current characteristics. The transience of the efficiency, stack consumption, and utilization are associated with the transience of the flow rates. After ~0.1 seconds, the fuel characteristics settle to an effectively steady state.

4.2.3.3 Boost converter

The boost converter is a DC/DC boost converter that utilizes a pulse width modulator with a set duty cycle. The duty cycle used by the boost converter is constant, as the output voltage of the fuel cell is not expected to vary greatly with time due to the idealized operation of the fuel cell stacks and that the hydrogen fuel source will be constant provided that there is enough fuel to power the fuel cell. The frequency of the PWM is 10kHz. The duty cycle is 0.75. This allows for the voltage to be boosted from ~45V to ~480V so that the fuel cell can interface with the associated grid following inverter.

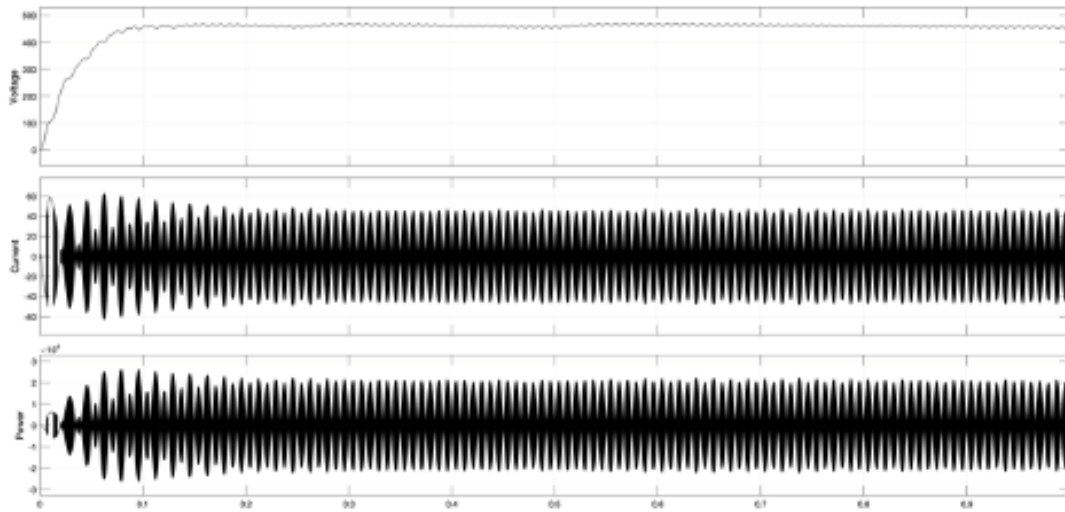


Fig. 27: Power, Current, Voltage out of Boost Converter

The voltage out of the boost converter increases to ~ 460 V to match with the input requirements of the grid-following inverter and is effectively DC. The voltage stabilizes within 0.1 second. The current characteristics behave in accordance to the grid-following inverter and become AC and stabilize within 0.2 seconds.

4.2.3.4 Hydrogen tank + electrolyzer

Both the hydrogen tank and electrolyzer are mathematical abstractions. The fuel tank calculates the used hydrogen based upon the flow rate of the input hydrogen vs time. A constant source can be set to indicate the initial amount of hydrogen that is stored within the tank. Once the hydrogen supply drops below the required amount of hydrogen to supply the fuel cell stacks for one second of operation, an output signal is sent to shut off the fuel supplied to the fuel cell stacks. The tank also takes in a hydrogen input from the output of the electrolyzer/hydrolyzer block. The electrolyzer/hydrolyzer gives a simple output of hydrogen/second if the input voltage and current are sufficient enough to turn on the electrolyzer.

4.2.4 Battery simulation

4.2.4.1 Battery model

The battery model is a component from the Simscape library which can be installed in Simulink. The battery used in this model is an ideal Lithium-ion, with rated capacity of 1000 Ah for energy storage for 12kW load. Details of the battery model is shown in table 7 below.

Table 7: Battery model parameters

Parameters	Value
Nominal Voltage	43.2 (V)
Rated Capacity	1000 (Ah)
Initial state-of-charge	70 (%)

The above parameters can be used to calculate the capacity of the battery model using the equation:

$$E = VIt$$

Where

E : Energy stored in battery model (W)

V : nominal Voltage (V)

It : Rated capacity of battery (Ah)

Based on the equation above, the battery can sustain a 12kW load for 3.6 hours

4.2.4.2 Buck/Boost converter

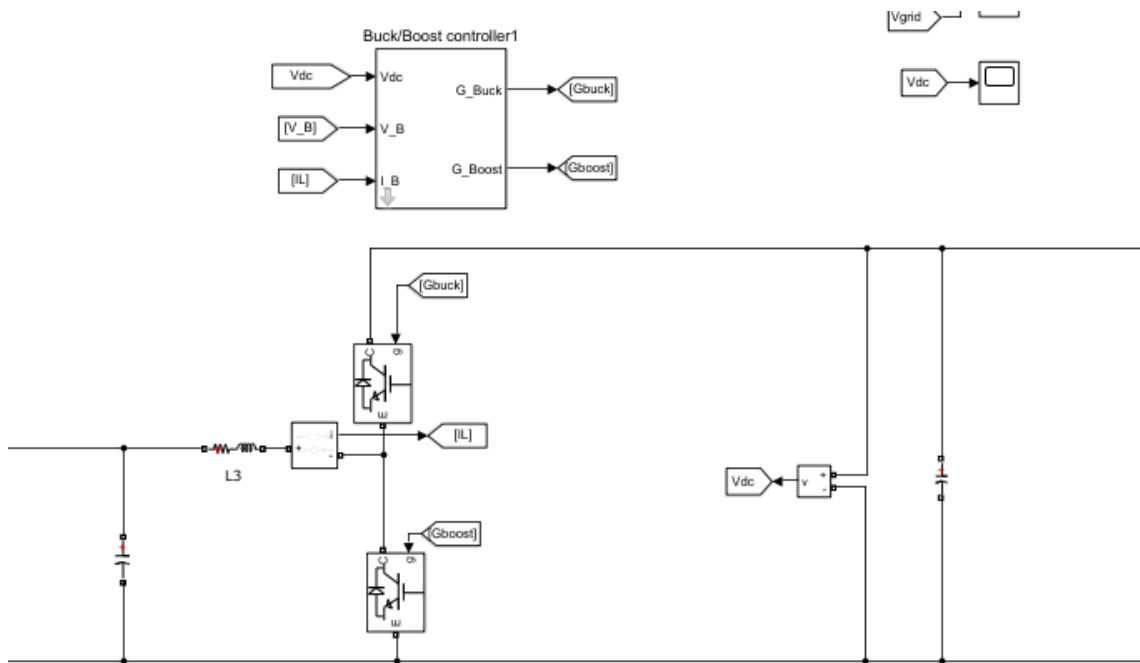


Fig. 28: Bidirectional DC/DC converter with control

The DC/DC converter works as a Boost converter when the battery is working discharge mode. The Boost converter voltage equation is as below:

$$\frac{V_{dc}}{V_b} = \frac{1}{1-D}$$

Where V_{dc} is the output DC link voltage, V_b is the battery output voltage and D is the duty cycle for the IGBT.

Likewise, when the battery is in charged mode, the DC/DC converter works as a Buck converter. The Buck converter voltage equation:

$$\frac{V_{dc}}{V_b} = \frac{1}{D}$$

The controller will decide the mode of charge or discharge based on the current input into the inverter. If this current is positive, then the battery should be working in discharge mode.

Otherwise, the battery will be working in charge mode.

5 Testing

Simulations will be broken into 6 sections.

1. Photovoltaic arrays
2. Wind Turbine
3. Hydrogen fuel cells
4. Inverters
5. Battery Storage
6. Controls

Each simulation will use realistic input data respective to our required deployment location, Kossuth County, IA. The simulations focus on transient behaviour of the system under each condition. These simulations will then be combined and the final output will be analyzed to ensure requirements are met.

Each individual component will be tested to ensure its requirements are met. Components will then be combined into systems, and each system will be tested.

5.1 MICROGRID TESTING/SIMULATION

Matlab/Simulink simulation is divided into 5 units:

- Solar panels & MPPT control: Ensure maximum power output under various irradiances.
- Wind turbine: Output 240V/60Hz AC power according to wind speed.
- Battery Energy storage system (BESS): Test charge and discharge mode. Modeling batteries' conditions (state of charge, stable DC voltage output)
- Inverters: Outputting 240V/60Hz AC voltage with various DC input.
- Hydrogen fuel cells

Each simulation unit is subjected to testing.

The process for microgrid simulation tests consisted of running time domain simulations of the electrical and/or electrochemical performance of the various components in isolation and in conjunction with each other. The differential equation solver ODE23S is used to conduct the simulations. Typical run times for these simulations are between 2 and 10 seconds. The key characteristics for each individual component that defines system performance are the internal and output voltages and currents as functions of time. The performance of the hydrogen fuel cells are also characterized by fuel consumption and stack efficiency as functions of time. Each energy generation source is paired with the described grid following inverter.

Table 8: Event for interconnected simulation.

Time	Event
t = 0 sec	1kW load, Battery/Grid forming Inverter is on
t = 0.2 sec	5kW load is added, total load is 6kW
t = 0.5 sec	Wind turbines is on
t = 0.8 sec	PV arrays is on
t = 1.2 sec	Hydrogen fuel cell is on
t = 2 sec	6kW load is added, total load is 12kW

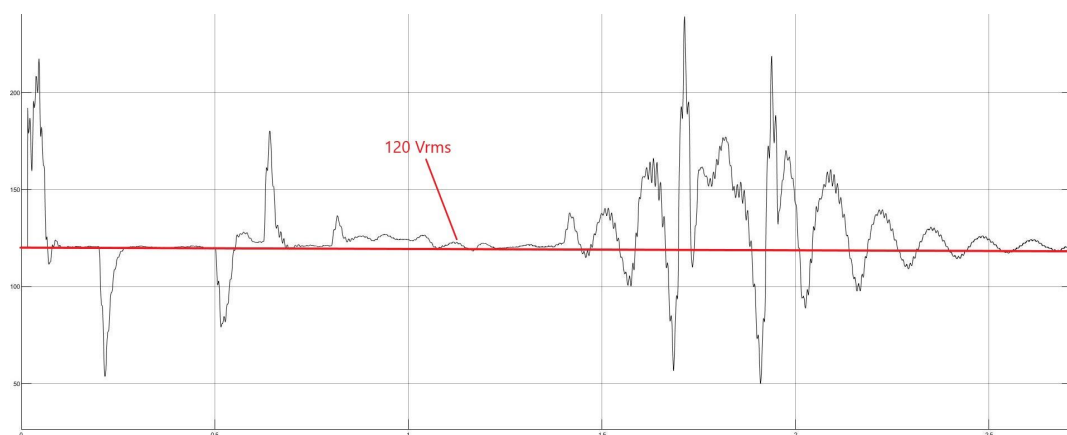


Fig. 29: RMS value of the output voltage of the system

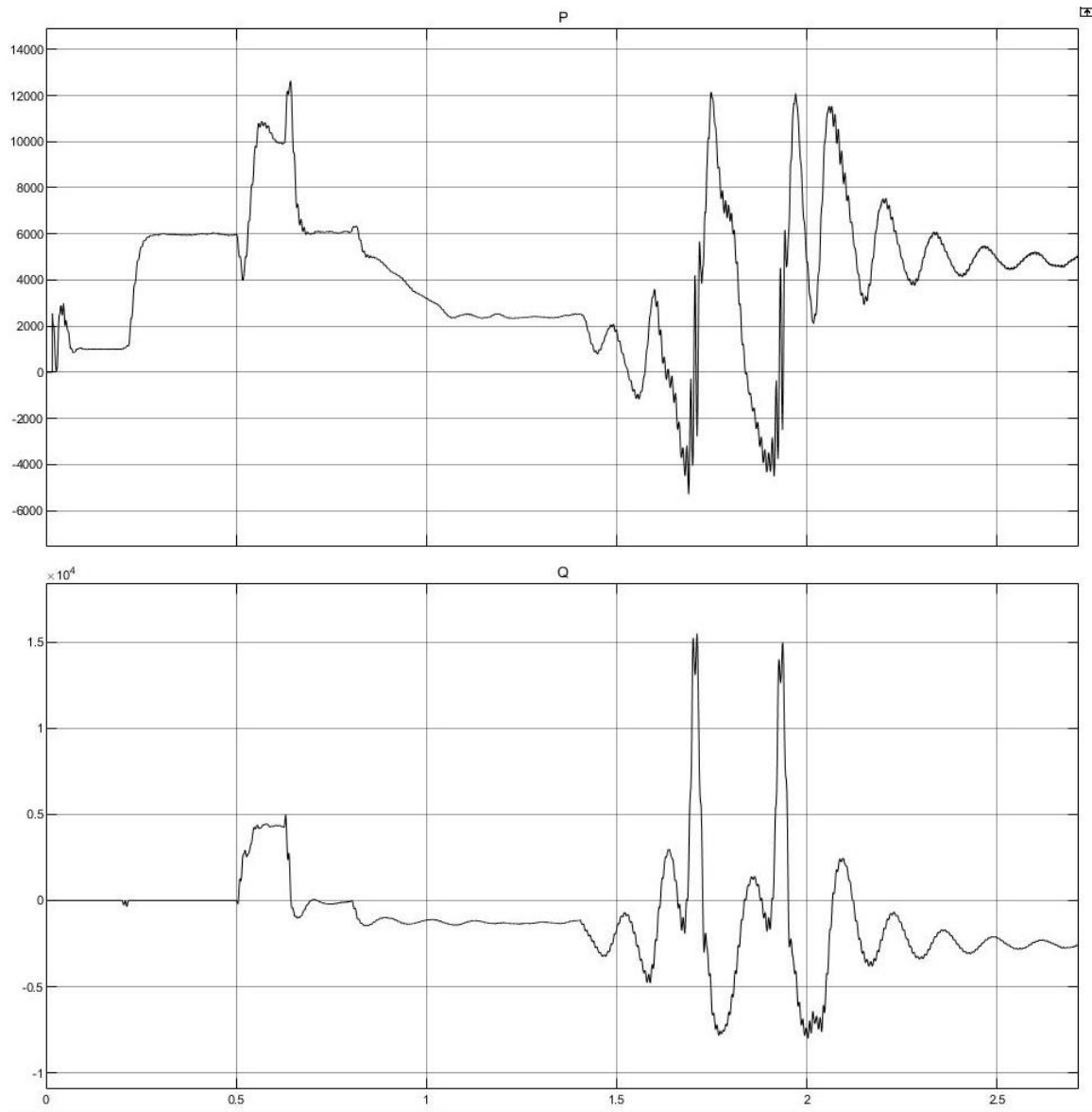


Fig. 30: Real and Reactive power of the model

Just like the voltage output magnitude, the real and reactive power initially fluctuates when at time where a new source of generation or a new load is introduced. Ultimately, the real and reactive power both settle to $P_{batt} = 5 \text{ kW}$ and $Q_{batt} = 2.5 \text{ kVar}$.

5.1.1 PV array model plots

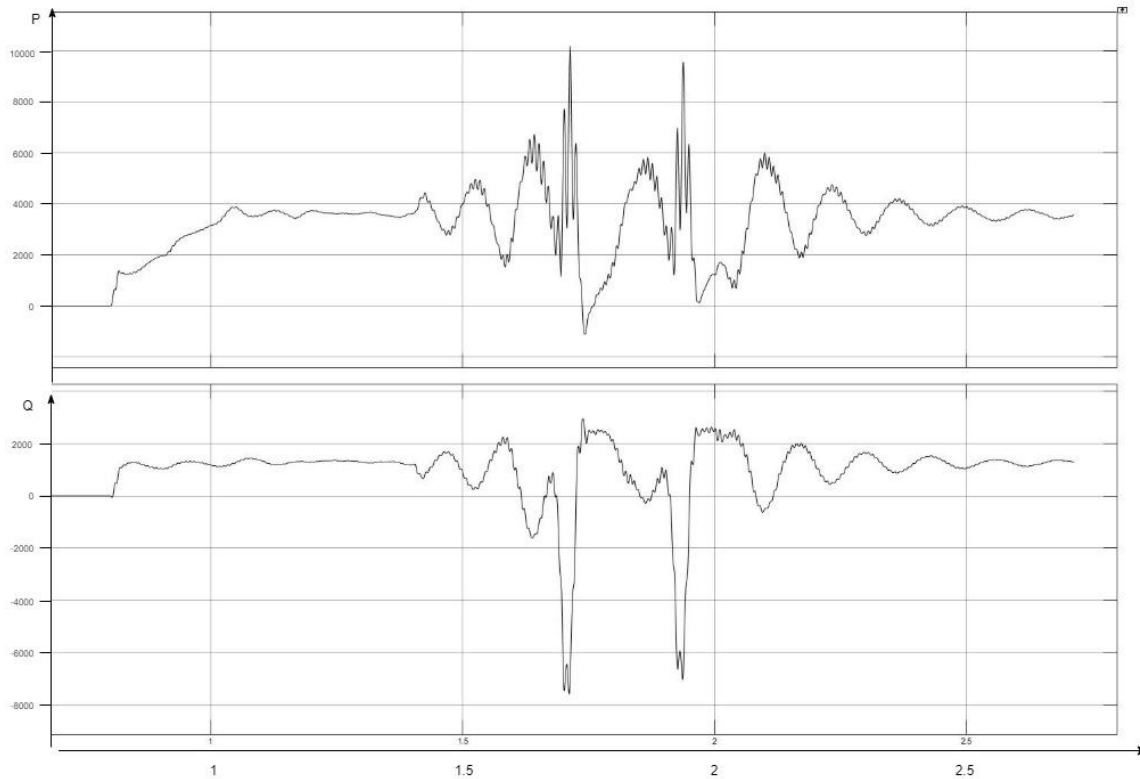


Fig. 31: Real and Reactive power plots for PV arrays

The PV array is switched on at 0.8 s and reaches stability fairly quickly. The system reaches a steady state at around 1.2 s where $P_{PV} = 3.9$ kW and $Q_{PV} = 1.5$ kVar. Ultimately, after the system is on and running at full load, P_{PV} and Q_{PV} return to the values above.

5.1.2 Wind Turbines model plots

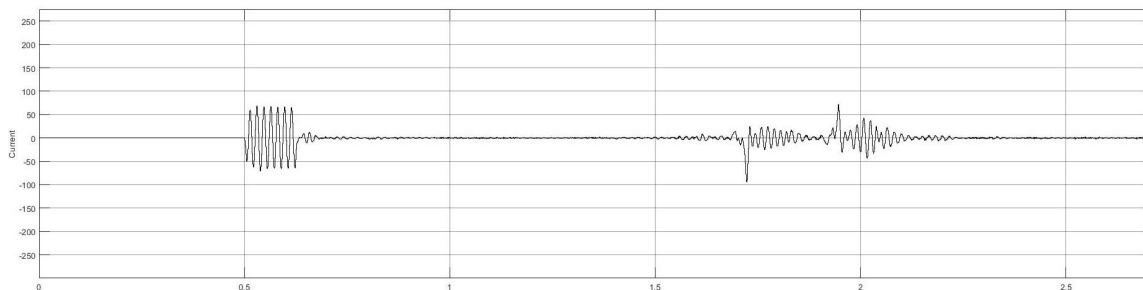


Fig. 32: Wind turbine output current

The wind turbine is switched on at 0.5 s. However, due to it being the first model to be initiated, the wind turbine settled fairly quickly. The output current of the wind turbine model is shown in Fig. 32. Examine closely, the wind turbine's output current goes to zero at 0.8 s, around the time when the PV array is introduced to the system. This is because the PV array itself and the battery's power

are sufficiently large enough to provide for the load. When the hydrogen fuel cell is being introduced to the system at 0.2 s, we can see that the current fluctuated a little bit as the inverters are trying to stabilize the output voltage of the systems. Eventually, when the voltage stabilizes, it returns to zero.

5.1.3 Hydrogen Fuel Cells model plots

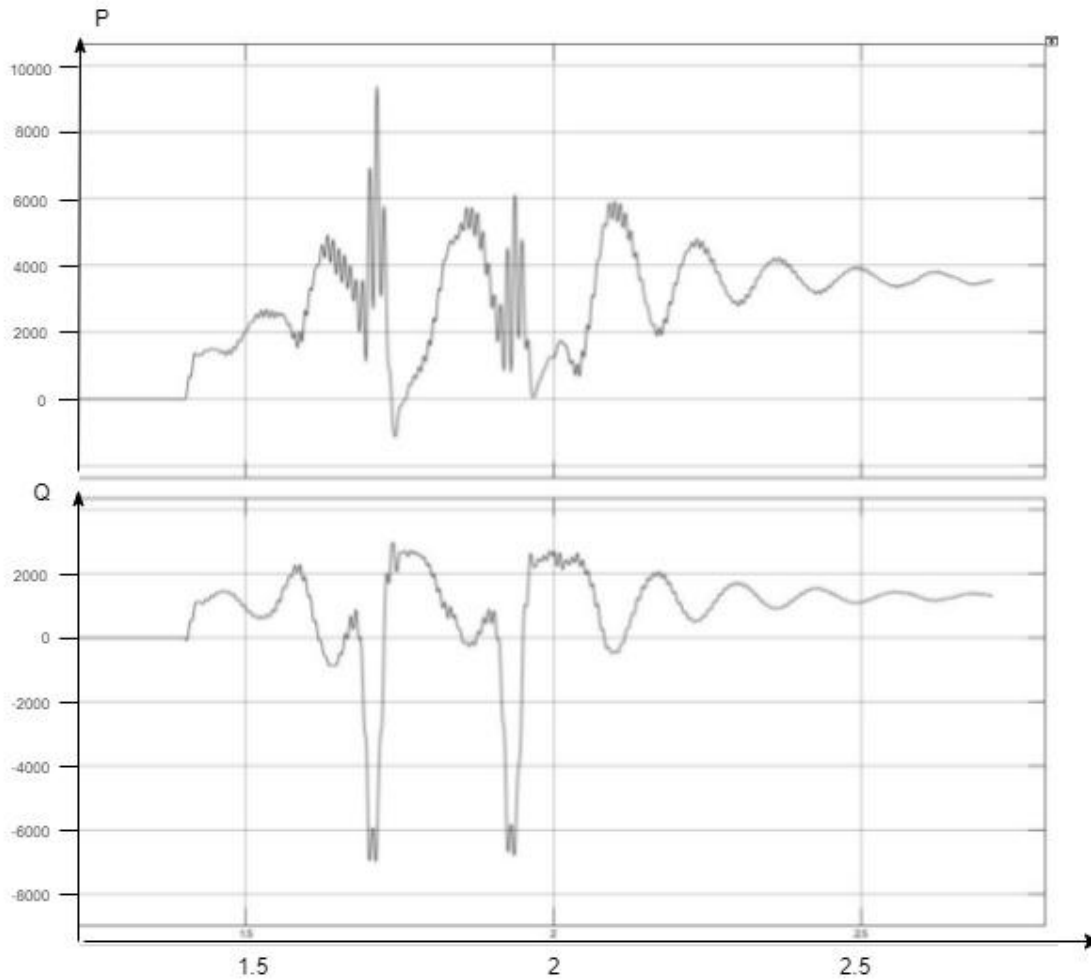


Fig. 33: Real and Reactive power output of the hydrogen fuel cell stack

The fuel cell stack is switched on at 1.4s and settles slowest. It took about 1 s for the whole system to stabilize at 2.4s. Finally, after the system is on and running at full load, P_{fc} and Q_{fc} steady state is at

$$P_{fc} = 3.9 \text{ kW and } Q_{fc} = 1.6 \text{ kVar.}$$

5.2 NANOGRID TESTING

The nanogrid is divided into three units.

1. Solar array (Jackery SolarSaga 100)

2. Battery/inverter system (Jackery Explorer 500)
3. Hydrogen Fuel cell (G-HFCS-30W6V)

The solar array being tested is the Jackery SolarSaga 100. This solar array was chosen because it is easily integrated with the Jackery Explorer 500 battery/inverter system. Even though the solar array and battery/inverter system can be viewed as separate units, much of our testing involved them being integrated. The battery/inverter system has a display capable of showing the output power of the solar panel charging the battery. This power display was verified using the following method. A cable capable of connecting the solar array to the battery/inverter system was cut. The insulation covering the positive and negative feeds was stripped back slightly. The leads from the positive feeds were connected to an ammeter. The negative leads were reconnected with a wire nut. This allowed a probe from a voltmeter to touch the conductor without danger to the person conducting the test. The second voltmeter probe was connected to the positive feed. All exposed wire was then covered with electrical tape. This cable was then used to connect the solar array to the battery. The voltage and current measurements from the voltmeter and ammeter were used to verify the battery display. Multiple tests were performed on the solar array and battery/inverter. Details on how these tests were/can be performed may be found in Appendix I.

Solar panel and battery system test results obtained by varying how many solar cells are receiving sunlight are shown in table 6.



Fig. 34: Nanogrid experiments- field tests and functionality testing

Table 9: Solar panel and battery performance tests

Partial coverage (# of cells covered out of 32)	Power Displayed (W)	Current Measured (A)	Voltage Measured (V)	Power Calculated (W)
0	64	3.75	18.12	68
2	37	3.1	11.28	35
4	17	1.35	11.14	15
8	9	0.8	11.1	9

Tests of the hydrogen fuel cell stacks were conducted in the lab of Dr. Wenzhen Li with the assistance of PhD student Hengzhou Liu. A Scriber fuel cell test station was utilized to perform tests of the voltage, current, and power characteristics of the fuel cell stack. This test station allows for control of the dew point of hydrogen, flow rate control, control of hydrogen pressure, sweeping of current density, and plotting of various key characteristics of the hydrogen fuel cell stack. Further details of the testing procedures are listed in Appendix I-3.

Various anode gas compositions were tested to determine an appropriate composite balance. The highest performing anode gas composite had a balance of 70% Hydrogen and 30% Argon. Figure 34 and figure 35 show plots of the voltage and power characteristics of the fuel cell stack when operating with the mentioned gas composition. A maximum power of 25.7 W was achieved with this gas configuration, which is 85.67 % of the specified operating value. The internal circuitry of the fuel cell stack prevented operation beyond this point, as the current had reached its maximum operating point of 5 A. The next set of tests conducted were to determine the impact of anode humidification on the output power. Anode gas dew point of 50 deg Celsius yielded a maximal power of 29.99 W. The increase in power was resultant of the decrease in membrane resistance due to the higher humidification associated with a higher anode gas dew point.

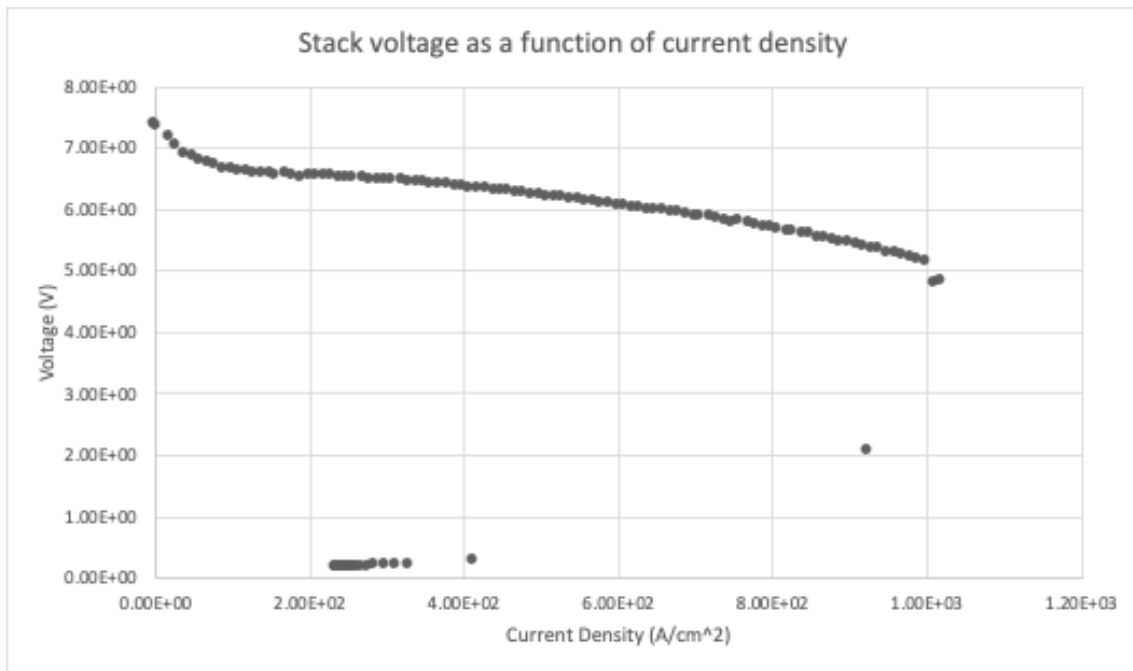


Fig. 35: Stack voltage as a function of current density

The voltage of the stack decreases accordingly with increases in current density. This characteristic is a primary determinant of the quality of the fuel cells assembly, materials used, and ware. The voltage of the fuel cell bottoms out after the current reaches 5 A due to the protective control circuitry of the fuel cell stack.

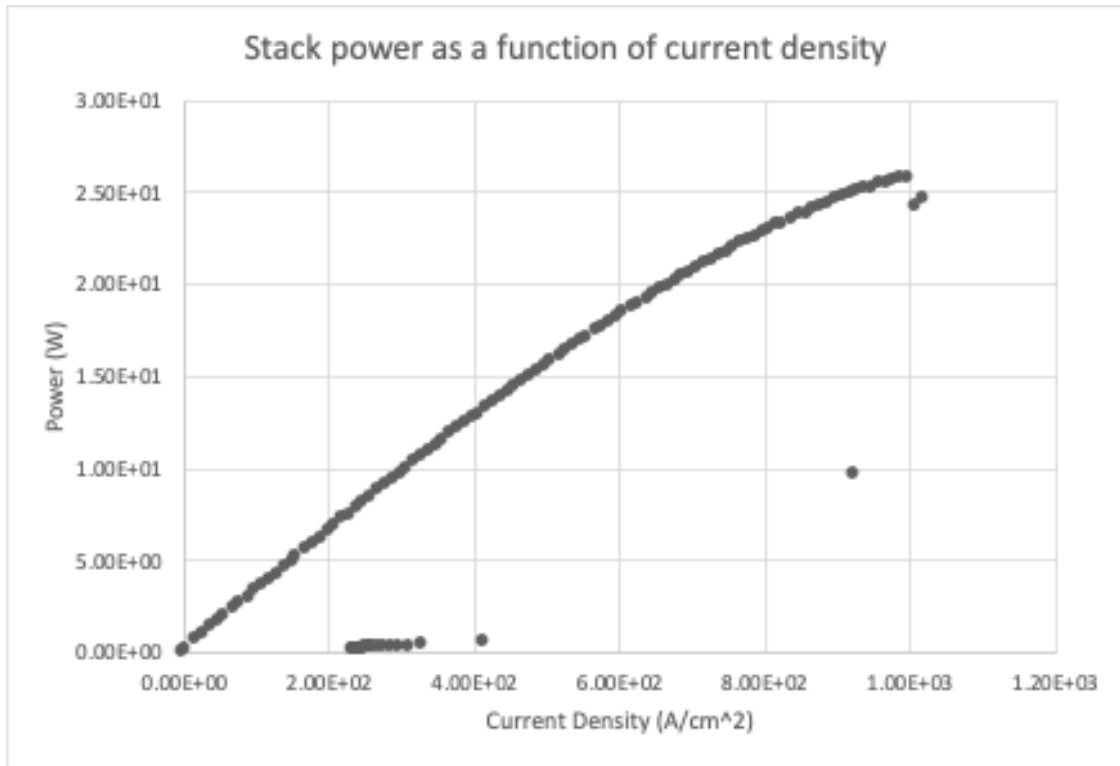


Fig. 36: Stack power as a function of current density

The stack power of the fuel cell stack increases linearly with current density until $\sim 400 \text{ A/cm}^2$ is reached. After this point, internal power loss due to mass transport limitations grow increasingly. Throughout all current densities, power losses occur due to internal cell resistance from humidity levels. The output power is limited by the protective control circuitry of the fuel cell stack.

6 Closing Material

6.1 CONCLUSION

Our simulations indicate that it is feasible to power a 12 kW constant load with a fully renewable microgrid that fits fully within a standard 20' shipping container. The configuration consisted of a PV array, wind turbine, hydrogen fuel cell system, battery, and inverters. Transients occur at the moment each component is connected to the system; however, the inverter controls stabilize the system output voltage to desired output.

The power output of each component was selected to enable the simulation of all the generation sources. However, these dimensions are subject to change depending on the required load, location and the associated optimal sizing for that load. Since wind turbines typically take up a significant amount of space; depending on the use case and site location the wind subsystem can be downsized

to fit in the ISO shipping container. On the other hand, the dimensions of the Solar PV array and fuel cells can be increased to maintain constant supply to the load.

Our testing of the nanogrid indicates similar findings. Our maximum output from the solar panels was approximately 70 Watts, while our maximum output from the hydrogen fuel cell was approximately 30 Watts. The solar panel we used was approximately 3 feet by 5 feet by 2 inches, while the hydrogen fuel cell was approximately 4 inches by 5 inches by 2 inches. Given that these are linearly scalable, and assuming an equal number of panels and fuel cells, we would need 60 solar panels and 60 fuel cells to power a 12 kW load. These would take up approximately 156 cubic feet of space. A standard ISO 20 shipping container has approximately 1,150 cubic feet of space available [11]. This means we would still have nearly 1,000 cubic feet of space available for a wind turbine, inverters, and battery.

6.2 REFERENCES

- [1] A. Banerji et al., "Microgrid: A review," 2013 IEEE Global Humanitarian Technology Conference: South Asia Satellite (GHTC-SAS), Trivandrum, 2013, pp. 27-35
- [2] R. P. Saini and S. Pant, "Comparative Study of MPPT Techniques for Solar Photovoltaic System," *IEEE Xplore*, 2019.. Available: <https://ieeexplore.ieee.org/abstract/document/8980004>.
- [3] Chauhan, Rajeev Kumar, and Kalpana Chauhan. *Distributed Energy Resources in Microgrids: Integration, Challenges and Optimization*. 1st ed., Academic Press, 2019.
- [4] A. Hirsch et al, "Microgrids: A review of technologies, key drivers, and outstanding issues", *Elsevier Renewable and Sustainable Energy Reviews*, Elsevier, July 2018, Vol 90, pp 402-411
- [5] J. Jiao, R. Meng, Z. Guan, C. Ren, L. Wang and B. Zhang, "Grid-connected Control Strategy for Bidirectional AC-DC Interlinking Converter in AC-DC Hybrid Microgrid," 2019 IEEE 10th International Symposium on Power Electronics for Distributed Generation Systems (PEDG), Xi'an, 2019, pp. 341-345, doi: 10.1109/PEDG.2019.8807601.
- [6] G. B. Arjun Kumar, Shivashankar and B. Shree Ram, "Hybrid PV - Wind Driven Generator Supplying AC/DC Microgrid for Rural Electrification," 2018 3rd IEEE International Conference on Recent Trends in Electronics, Information & Communication Technology (RTEICT), Bangalore, India, 2018, pp. 2283-2287, doi: 10.1109/RTEICT42901.2018.9012328.
- [7] "IEEE Standard for the Specification of Microgrid Controllers," in *IEEE Std 2030.7-2017*, vol., no., pp.1-43, 23 April 2018, doi: 10.1109/IEEESTD.2018.8295083.
- [8] M.M. Rahman, A. T. Al Awami, A.H.M.A. Rahim, "Hydro-PV-Wind-Battery-Diesel Based Stand-Alone Hybrid Power System," *ICEEICT 2014*
- [9] M. Larrañaga Aizpurua and Z. Leonowicz, "Advanced Solar Energy Systems with Thermoelectric Generators," 2018 IEEE International Conference on Environment and Electrical Engineering and

- 2018 IEEE Industrial and Commercial Power Systems Europe (IEEEIC / I&CPS Europe), Palermo, 2018, pp. 1-4, doi: 10.1109/IEEEIC.2018.8493685.
- [10] A. Urtasun, P. Sanchis and L. Marroyo, "Small Wind Turbine Sensorless MPPT: Robustness Analysis and Lossless Approach," in IEEE Transactions on Industry Applications, vol. 50, no. 6, pp. 4113-4121, Nov.-Dec. 2014, doi: 10.1109/TIA.2014.2313650.
- [11] Structures, Falcon. "Shipping Container Dimensions & Sizes: 40 Ft, 20 Ft, 10 Ft." *Shipping Container Dimensions & Sizes | 40 Ft, 20 Ft, 10 Ft*, www.falconstructures.com/shipping-container-dimensions.
- [12] "Alpha-Beta-Zero to dqo, dqo to Alpha-Beta-Zero." *Perform Transformation from $\alpha\beta\theta$ Stationary Reference Frame to dqo Rotating Reference Frame or the Inverse - Simulink*, www.mathworks.com/help/releases/R2020b/physmod/sps/powersys/ref/alphabetazerotodqodqotoalphabetazero.html#btrj7zv-3.
- [13] "Permanent Magnet Synchronous Machine," Three-phase permanent magnet synchronous machine with sinusoidal or trapezoidal back electromotive force, or five-phase permanent magnet synchronous machine with sinusoidal back electromotive force - Simulink, 2021. [Online]. Available: <https://www.mathworks.com/help/physmod/sps/powersys/ref/permanentmagnetsynchronousmachine.html>. [Accessed: 23-Apr-2021].
- [14] K. Anderson, E. Hotchkiss, L. Myers, and S. Stout "Energy Resilience Assessment Methodology" *National Renewable Energy Laboratory*, Oct. 2019
- [15] "Lazard's Levelized Cost of Storage Analysis - Version 4.0" *Lazard* Nov. 2018

Appendix I - Operation Manual

This project consisted of two aspects; simulating a microgrid, and testing a nanogrid.

NANOGRID

Setting up and testing the nanogrid should be accomplished in the following steps.

1. Attaching the solar panel to the battery.
 - a. For best results, ensure the solar panel is in a sunny area.
 - b. Use a barrel connector to connect the solar panel to the battery. The barrel connector should have the following dimensions.
 - i. 7.9 mm outer diameter
 - ii. 5.55 mm inner diameter
 - iii. 11 mm length
 - iv. 0.9 mm pin thickness
2. Testing the solar panel and battery

- a. Record the time, date, and location of the test.
- b. Use the information to obtain the available solar irradiance.
- c. There are multiple tests that can be run involving the solar panels.
 - i. Testing solar power output variance over a period of time.
 1. The battery has a display showing the power input. Record this value at the beginning of your test.
 2. Wait a set period of time (For most of our tests, we used 5 minute intervals).
 3. Record the power input from the battery display.
 4. Repeat this process for as long as desired.
 - ii. Testing solar power output while varying the number of solar cells receiving sunlight.
 1. The solar cell array has 32 cells. Leave all cells uncovered and receiving sunlight.
 2. Record the power input with all cells receiving sunlight.
 3. Then cover one cell (this may be done effectively with a piece of cardboard).
 4. Record the power input.
 5. Cover two cells.
 6. Record the power input.
 7. Cover four cells.
 8. Record the power input.
 9. Cover eight cells.
 10. Record the power input.
 - iii. Testing battery output while varying the load.
 1. Attach a load to one of the outputs of the battery. A good option is a multi-speed fan powered from the AC output of the battery system.
 2. Record the power output.
 3. Vary the load (with a multi-speed fan, this can be done by changing the fan speed).
 4. Record the power output.
 5. Repeat this process.

6. Verify the power output matches the expected power based on the load characteristics.
3. Testing the hydrogen fuel cell stack:
 - a. connect the fuel cell stack to the Scriber fuel cell test station:
 - i. connect the hydrogen tube to the hydrogen input of the fuel cell. For our fuel cell, you do not need to connect the oxygen terminal.
 - ii. connect the output voltage terminal of the fuel cell to the voltage and current sensor of the test station
 - b. Turn on the fuel cell test station:
 - i. open the valves of 3 gas tanks: hydrogen, nitrogen and argon. The station requires all 3 gas to work.
 - ii. on the software of the computer attached to the test station, input the fuel cell parameters such as number of cells, pressure of hydrogen, membrane area.
 - iii. select the current range you would like to test the fuel cell on, the temperature of the input gas. Click OK
 - iv. See if there are any voltage output from the fuel cell. If not observing any voltage, consider the sensor's connection again or contact Dr. Li for help.
 - v. Click apply load to begin testing. Make sure to save plots and data for later analysis.

SIMULATION

Running and testing the microgrid simulation

1. The generation sources (solar PV, wind turbine and hydrogen fuel cell) should all be connected to a total of 12kW resistive load, Each generation source is capable of powering a significant portion of the load. Therefore to observe the performance of all the sources circuit breakers are needed to allow each source to be introduced and settle.
2. When the simulation is run
 - a. Wind Turbine is switched on and 0.5s, some transient behavior is expected, but steady state should be reached fairly quickly.
 - b. At 0.8s the PV array is introduced, and Wind Turbine is switched off. Some transient behavior is expected. PV array takes slightly longer than Wind Turbine to reach steady state, but still fairly quick.
 - c. At 1.4s the Hydrogen fuel cell is introduced. The fuel cell takes the longest to reach steady state.

3. To observe each systems individual performance
 - a. Select system block.
 - b. Select PQ scope to observe real and reactive power plots.
 - c. Select VI scope to observe current and voltage plots.
4. To observe overall system performance. Since all generation sources are connected to the battery.
 - a. Select Battery system block
 - b. Select VI, PQ scope, this scope produces RMS voltage and current plots, as well as real and reactive power plots for the time horizon of the simulation.

Appendix II - Initial design

The first time when we try to interconnect all of the individual models, it takes a very long time to run the simulation (roughly 12 hours of run time). This leads to the realization that we need to establish the grid before connecting it to the grid following inverters. That is each time a new component (eg. a load or source of generation) is introduced into the system, make sure we have at least 0.4 seconds of simulation time before introducing the next component. This makes sure that the grid forming inverter or grid following inverter has fully passed its transient state.

It is also advised by our advisor that we take a step back and try to integrate each component one by one at a time to make sure that every component is working together properly. Only after confirming that the component is working with the existing microgrid do we try to incorporate the next component model into the simulation.